The selectivity curves for the hydrocyclone operating with 4 and 6-mm inserted-rods comparing with that of operating without inserted-rod are presented in Figure 26. It can be seen that the hydrocyclone operating with the 4-mm inserted- rod can gives the best separation performance, while the operating with the 6-mm inserted-rod gives the worst separation performance. It can be concluded that the hydrocyclone separation performance can be improved by replacing the air core with the proper size of the inserted-rod. The negative effect on the separation found in the experimental study of Lee and Williams (1993) might be due to both the design of the inserted-rod body supports and the size of inserted-rod.

4.6. Conclusion

In conclusion, the Computational Fluid Dynamics (CFD) techniques to the simulation of 3D flow within a hydrocyclone operating with an air-core and with inserted-rod by using the Finite Volume Method (FVM) has been introduced. The particle motion was successfully predicted by using the particle trajectory method. The separation performance of the separator was determined by the relationship between percentages of the each particle size of feed reporting to the underflow discharge. The numerical results from this study were in good agreement with the experimental data. It was found that the radial and axial velocity components in the area that just below the vortex finder were reduced, when replacing the air core by inserting a metal rod. This causes the flow field inside hydrocyclone become more beneficial for the separation process. However, the separation performance can only be improved with the proper size of the inserted-rod. The reduction of pressure loss in the hydrocyclone was also found to be reduced by replacing the air core by inserting a metal rod.

5. References

Chu, L., Yu, W., Wang, G., Zhou, X., Chen, W. and Dai, G. (2004) Enhancement of hydrocyclone separation performance by eliminating the air core, *Chemical Engineering and Processing*, Vol. 43, Issue 12, pp. 1441-1448.

Concha, F., Barrientos, A., Montero, J., Sampaio, R. (1996) Air core and roping in hydro cyclones. *International Journal of Mineral Processing*, 44-45, 743-749.

Fisher, M., Flack, R. (2002) Velocity distributions in a hydrocyclone separator. *Experiments in Fluids*, 32, 302-312.

Gresho, P. (1991) Incompressible fluid dynamics: Some fundamental issues. *Annual Review of Fluid Mechanics*, 23, 413-453.

Haroutunian, V., Engelman, M. S. and Hasbani, I. (1993) Segregated finite element algorithms for the numerical solution of large-scale incompressible flow problems, *International Journal for Numerical Methods in Fluids*, Vol. 17, pp. 323-348.

Lee, M. S. and Williams, R. A. (1993) Performance characteristics within a modified hydrocyclones, *Minerals Engineering*, Vol. 6, No. 7, pp. 743-751.

Luo, Q., Deng, C., Xu, J. R., Yu, L. and Xiong, G. (1989) Comparison of the performance of the water sealed and commercial hydrocyclones, *International Journal of Mineral Processing*, Vol. 25, pp. 297-310.

Neesse, T., Schneider, M., Dueck, J., Golyk, V., Buntenbach, S., Tiefel, H. (2003) Hydrocyclone operation at the transition point rope/spray discharge. In: *Hydrocyclones 2004*, in South Africa.

Patankar, S. V. (1980) Numerical heat transfer and fluid flow, New York: Hemisphere Publishing Corporation, Taylor and Francis Group.

Xu, J., Luo, Q. and Qiu, J. (1990a) Studying the flow field in a hydrocyclone with no forced vortex, Part I - average velocity, *Filtration and Separation*, Vol. 27, pp. 181-182.

Xu, J., Luo, Q. and Qiu, J. (1990b) Studying the flow field in a hydrocyclone with no forced vortex, Part II- average velocity, *Filtration and Separation*, Vol. 27, pp. 356-359.

III. The experimental study of the flow within a hydrocyclone operating with an air core

1. Abstract

The experimental studies of the flow behaviour within 50-mm hydrocyclones with and without a vortex finder attachment (Fin) have been performed. The flow characteristics within both hydrocyclones were observed visually and recorded both photographically and on video as the hydrocyclones are made of a transparent material. The development of the double-helical flow was observed; also the shape and diameter of the air-core have been examined for different values of operating pressure drop. It was found that the air-core is unstable and its size, shape and position are unfixed because of the instability of the gas-liquid interface. The results also showed that the air core is related to the shape of the underflow discharge and is a function of the pressure drop. A regular spray discharge from the spigot was observed. The roping discharge was observed when an extension pipe was connected to the underflow outlet. An increase in pressure drop leads to an increase in air-core diameter and the angle of the underflow profile. However, the relationships between these three parameters are non-linear. The knowledge of the size and location of the air-core relative to the operating pressure drop can assist in the validation of computational fluid dynamics (CFD) simulation work.

The separation performance of these two transparent hydrocyclones for a CaCO₃ in water system has been investigated. In this study, the results showed that a fin-type vortex finder attachment could not increase the sharpness of separation but it could help in the thickening process. It can be seen that the separation performance does not depend only on the geometry and operating conditions, but also on slurry concentration and particle size distribution. The concentration of the feed slurry and the operating pressure drop strongly affect the sharpness of separation.

2. Introduction

Hydrocyclones are widely used in the mineral, chemical, coal, powder-processing industries for de-watering, or classifying according to a required particle size or density separation.

The reasons for this popularity lie in their simplicity of design and operation, high throughput, low maintenance, low operating cost and small physical size of the unit. Hydrocyclones are physically simple and robust separation devices with no moveable parts. A typical hydrocyclone consists of three sections; a cylindrical section, conical section and a tangential inlet section. The tangential inlet section is attached to the cylindrical section. The vortex finder is located centrally through the lid and at the top of the cylindrical section. Figure 1a shows a conventional hydrocyclone, which is inherently simple in construction. The design variables which influence the performance of the unit operation are the inlet and outlet diameters. The separation process is achieved as a result of the centrifugal force acting on the slurry and its components. However, there is a secondary flow down the outside wall of the vortex finder to the overflow, which is called a short-circuit flow. This flow was reported to cause low particle separation efficiency (Kelsall, 1952). Svarovsky (1994) suggested that a redesigned-vortex finder with a skirt can eliminate this inefficiency problem.

Despite its apparent simplicity, the elucidation of the mechanism of separation and detailed models of fluid flow with hydrocyclone separators has yet to be achieved. The main reasons for these short comings are: the complexity of solving Navier-Stokes equations for non-Newtonian anisotropic fluids that contain high concentrations of interacting particles, The complex high swirling and varying turbulence conditions prevailing in the separator, the presence of an interface (the air-core) inside the separator and the lack of on-online measurement methods to provide reliable experimental data for model development under credible process conditions (Bond et al., 1999).

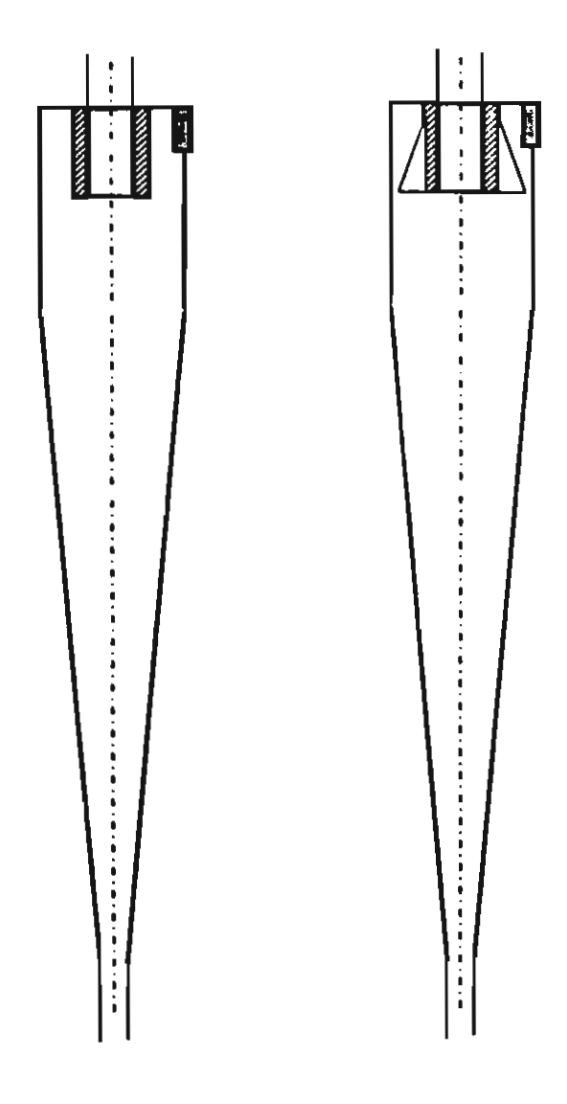
An attempt to model the flow in a hydrocyclone has been made by using a theoretical model, which is based on solving the Navier-Stokes equations. This approach provides a physical insight into the fundamental causes of the observed phenomena. The earlier theoretical models were presented by Bloor and Ingham (1973), (1975) and (1987), Pericleous and Rhodes (1986), and Hsieh and Rajamani (1991). These steady state and 2D-axisymmetrical models have been considered, but the results are limited to dilute flow only. In addition, it is difficult to describe the behaviour of high turbulent swirling flow caused by the 3D flow entry. Therefore, more advanced modelling is needed that allows,

for example, the study of such phenomena as an adjustment of three-dimensional flow to axisymmetrical, particle-fluid, particle-particle and particle-wall interactions. Such models will allow the description of particle effects on suppressing or generating turbulence and non-Newtonian slurry flows. Additionally, in the context of modelling turbulence, a physical model is needed to show how a fluid turbulent deformation characterises swirl flows and the deformation of the air-core inside the separator. Advanced theoretical and experimental techniques are needed to obtain a better understanding of the complex physical phenomena affecting the performance of hydrocyclones.

The purpose of this work is to study the flow behaviour, focusing on the air-core and underflow discharge characteristics, by using 50-mm transparent hydrocyclones with and without a vortex finder attachment (Fin). The experiments of these hydrocyclones treating CaCO₃ in water system are carried out. The knowledge of the underflow discharge characteristics relative to the operating pressure drop and feed property affecting the separation performance is investigated.

3. Experimental systems

Figure 1 shows the schematic diagram of both 50-mm diameter acrylic hydrocyclones with and without a vortex finder attachment. They were equipped and set up with a feed pump and pressure gauge to measure the feed inlet pressure (see Figure 2). The vortex finder and apex diameters were kept constant at 14mm and 10 mm. Hydrocyclone overflows and underflows were directed back to the sump for recirculation. To study the flow behaviour and the characteristics of the air core, water was used. The operating pressure drop was varied from 10 psi to 35 psi by varying the inlet water flow rate. The density and the viscosity of water are 1031 kg/m³ and 1.330 cp, respectively. The size and the location of the air core were observed relative to the pressure drop. From each experiment, samples were collected from the feed, overflow and underflow streams. The collected samples were weighed and mass flow rates determined.



(a)

Geometry	Value (mm)
underflow internal diameter	10
vortex finder internal	14
diameter	
vortex finder outer	28
diameter overflow	
cylindrical section diameter	45
conical section length	270
cylindrical section length	40
width of inlet orifice	22
length of inlet orifice	40
height of inlet orifice	16
length of fin	6
height of fin	20

Figure 1. Schematic diagram of 50-mm diameter acrylic hydrocyclones (a) conventional hydrocyclone and (b) with a vortex finder attachment (Fin).

(b)

The separation performance was examined by using the solution of CaCO₃ in water as feed slurry. The density of CaCO₃ is 2700 kg/m³. The flow rate and concentration of the feed was varied. In this case, the solid phase in each stream was also weighed to determine the concentration. The particle size distribution of each stream was measured by using the laser-diffraction size-analysis technique.

Overflow (return to sump)

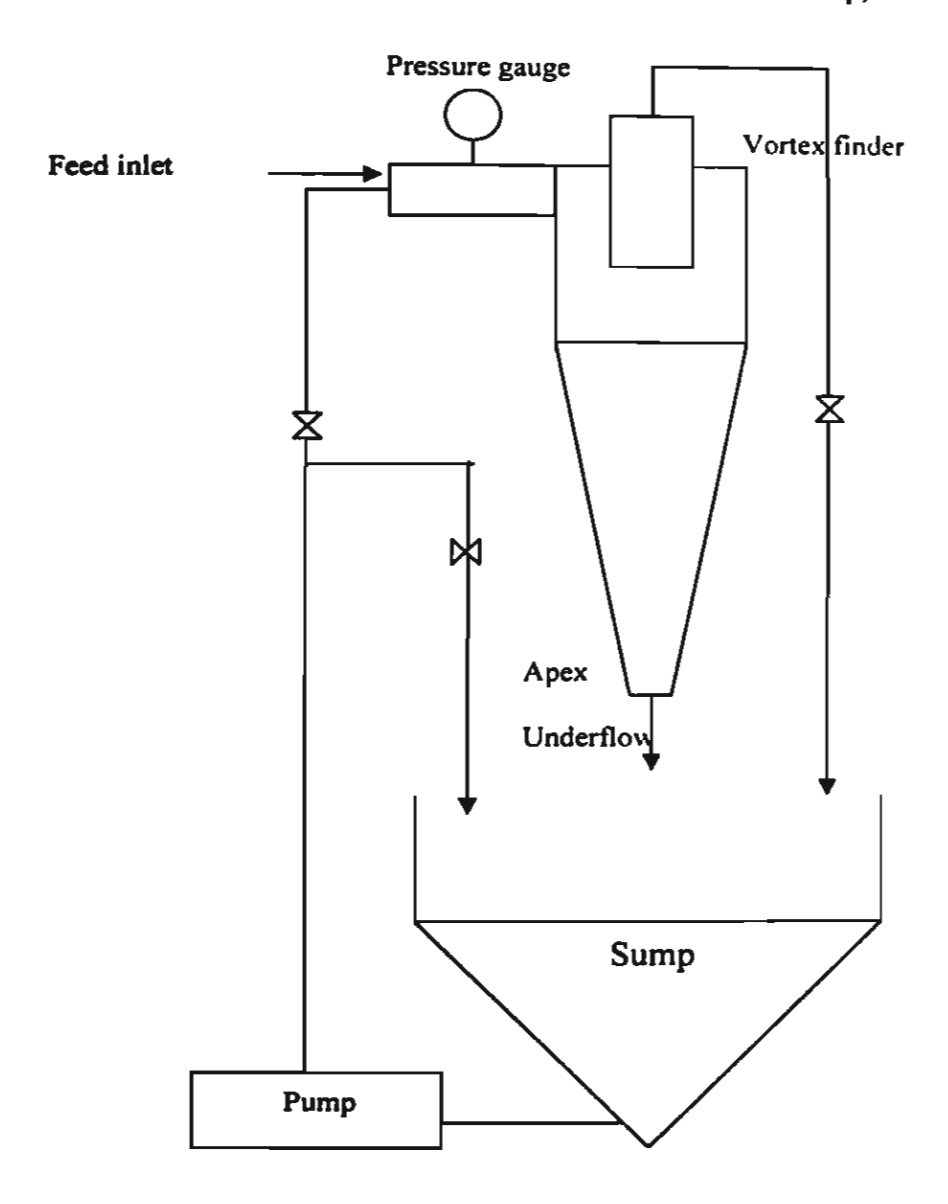
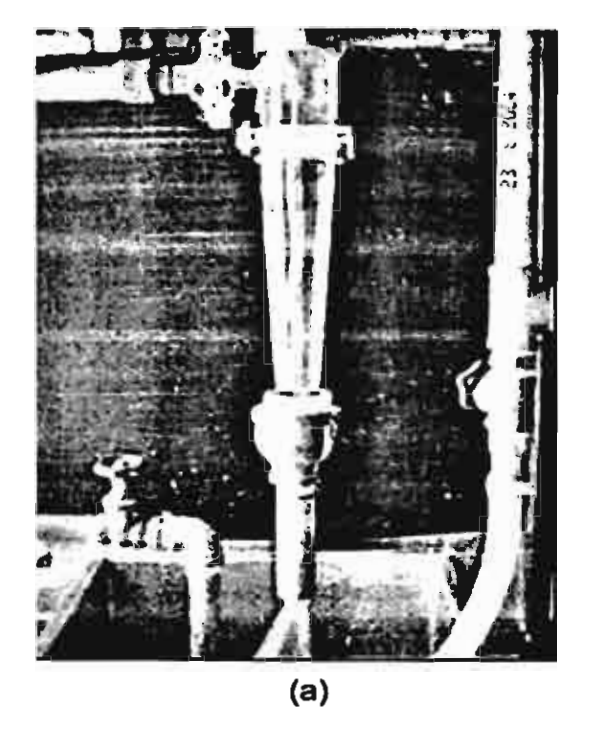


Figure 2. Hydrocyclone apparatus.

4. Flow behaviours

The diameter of the air-core of a conventional hydrocyclone for water-only flow was measured and found to be increased due to an increase in the pressure drop. It is also related to the angle of the underflow profile.



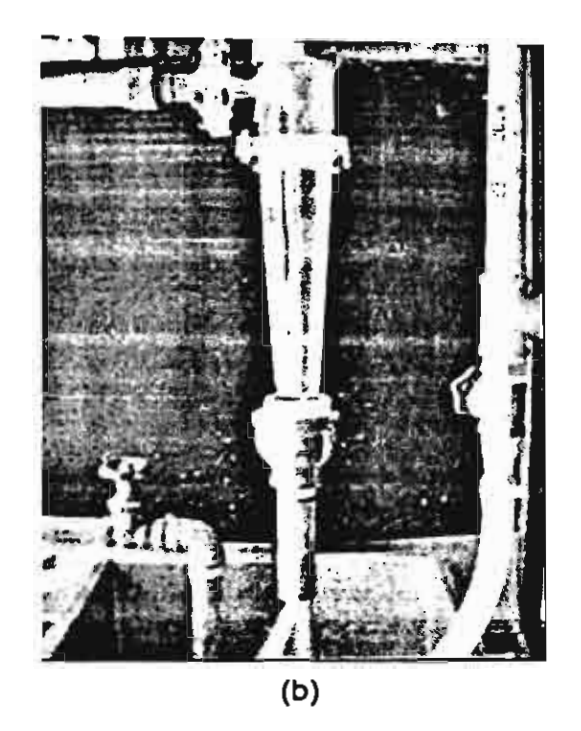
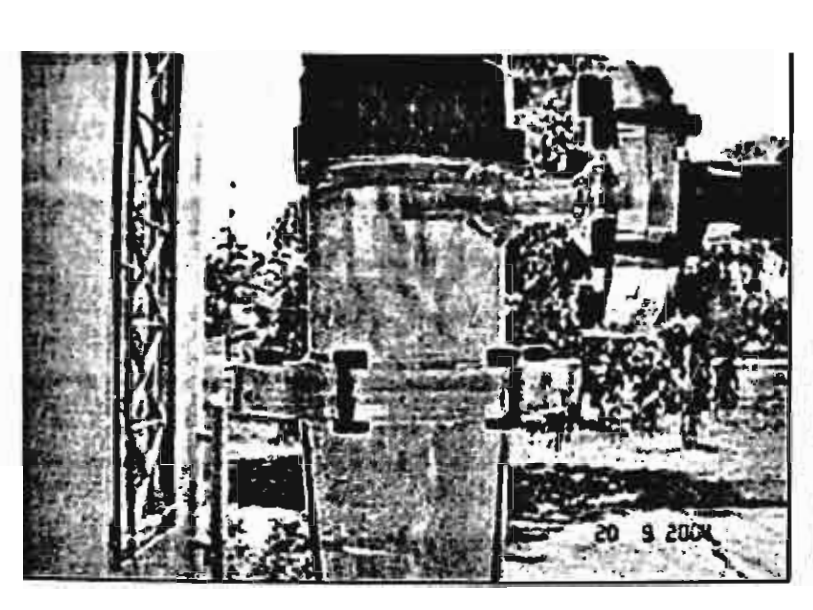
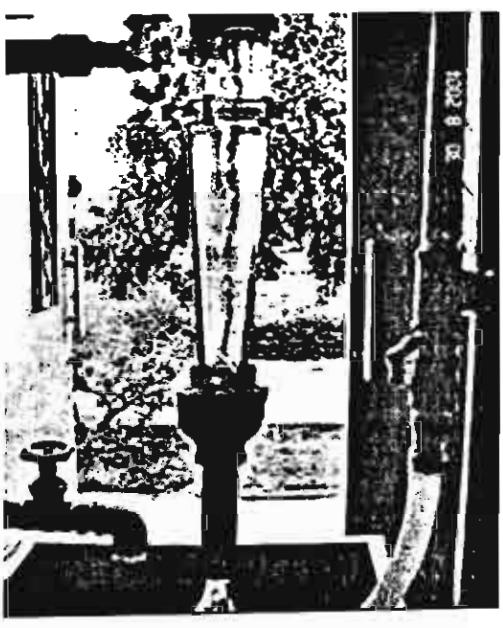


Figure 3. The flow pattern within the conventional hydrocyclone operating at: a) 10 psi b) 30 psi.





(a) (b)

Figure 4. The flow pattern within the hydrocyclone with a vortex finder attachment operating at 10 psi.

In addition, the angle of the underflow discharge of a conventional hydrocyclone treating CaCO₃ slurries was observed for 1%, 2% and 5% by volume of solid in feed as shown in Figure 5.

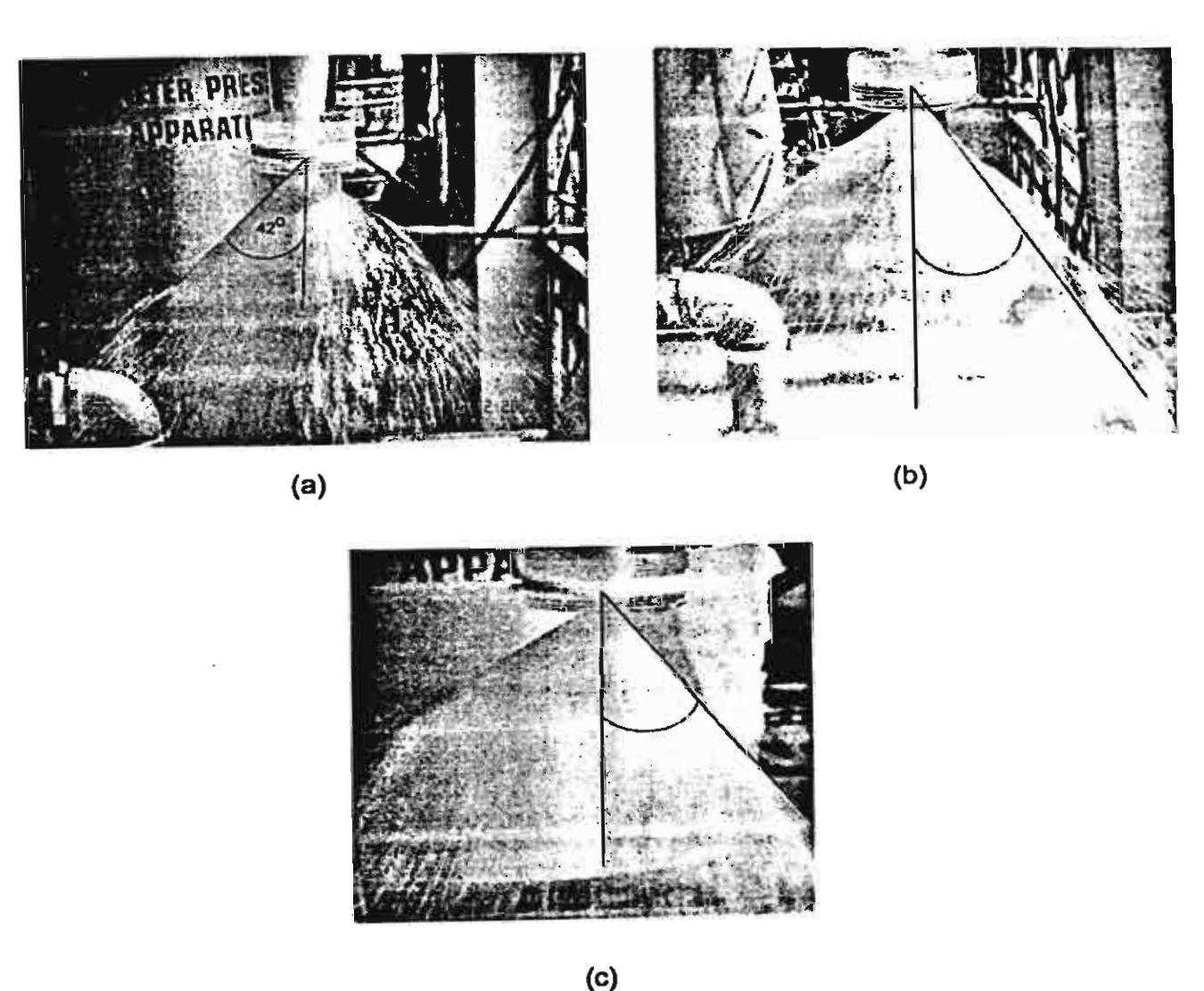


Figure 5. The underflow discharge of the hydrocyclone operating at 30 psi for feed solid concentrations of: a) 1% b) 2% and c) 5% by volume.

A regular spray discharge from the spigot was observed in every experiment. The shape of the underflow discharge was found to be altered according to the change of feed-solid concentration and operating pressure drop as shown in Figure 6. Figure 6 also depicts the relationships between the air-core diameter, the angle of the underflow discharge and the pressure drop. It was found that an increase in pressure drop leads to an increase in the air-core diameter. However, in low-solid concentration cases, which are 1 and 2% by

volume of solid in feed, it was found that an increase in pressure drop leads to an increase in the angle of the underflow profile. For higher solid concentration, which is 5% by volume, it was found that above a certain operating pressure (25 psi), the discharge angle decreases due to the increase in pressure drop. This is due to the sedimentation of solids in the underflow section caused by high operating pressure in dense-flow separation.

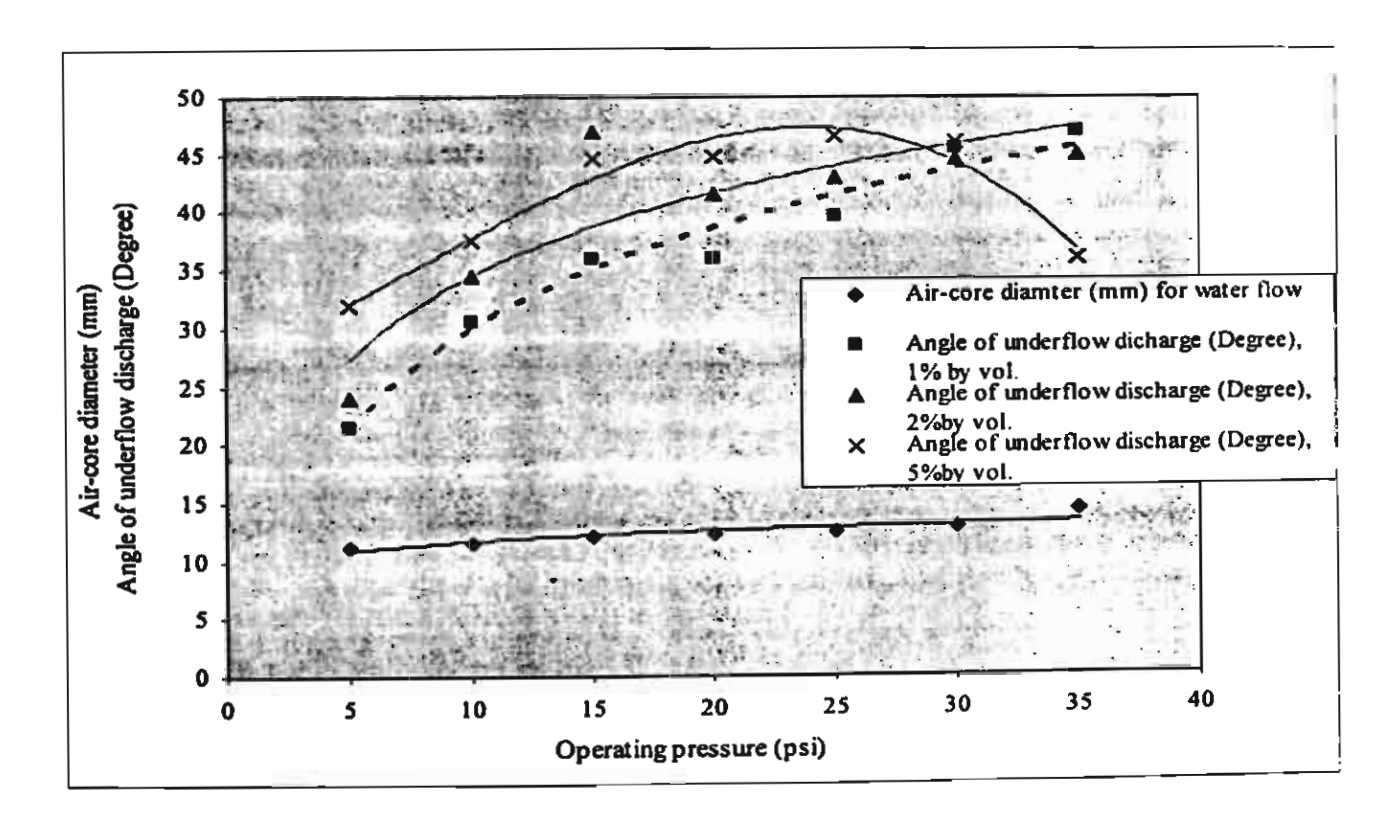


Figure 6. The relationship between the pressure drop, the air-core diameter and the angle of underflow discharge.

The solid concentration has a very strong effect on the angle of underflow discharge. The relationships between these three parameters are non-linear.

5. Separation performance

The separation performance of this hydrocyclone with the extension pipe, treating $CaCO_3$ slurry, was examined. The operational data (pressure drop), the concentration and flow rate of each stream, the cut size and throughput ratio (R_f) of each test are shown in Table 1.

The throughput ratio, R_{f} is the ratio between the volumetric flow rate of the underflow and that of the feed. The particle size distribution of the feed is shown in Figure 7. The selectivity curves are presented in Figures 8-11.

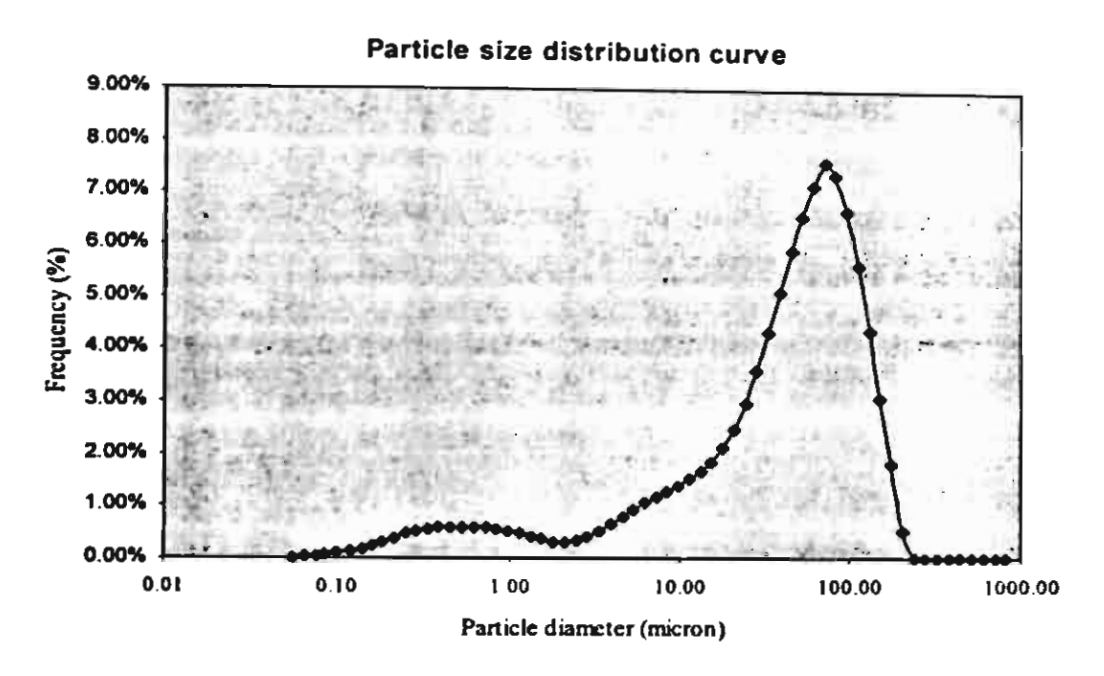


Figure 7. Particle size distribution curves.

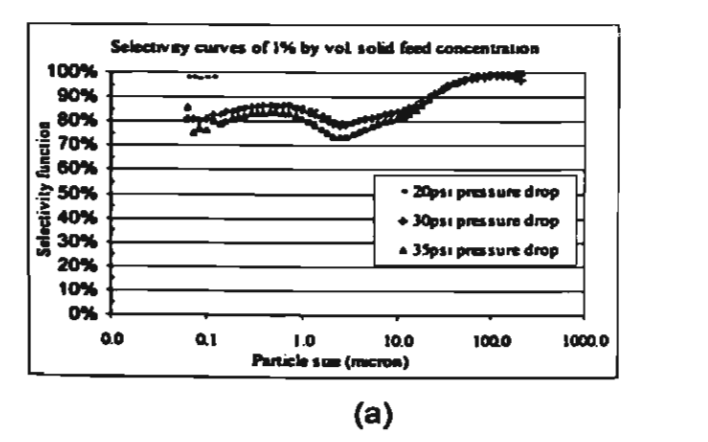
In this study, the operating pressure is limited. The highest pressure drop is 35 psi. In this range, it was found that the performance of the 50-mm hydrocyclone unit treating CaCO₃ slurry at 1 and 2% by volume was poor. The cut size cannot be obtained as can be seen in Figure 8a and 8b. However, the solid concentration in the underflow was three times higher than the concentration in the feed. The separation performance of the hydrocyclone treating the feed in this concentration range could be improved for a higher pressure drop.

The selectivity curves of the operation at the feed concentration of 5% by volume are shown in Figure 9. The separation performance of the hydrocyclone on this feed solid concentration is good. The results showed that the operating pressure of 35psi gave the smallest cut size. It is shown that the change in pressure drop obviously affects the hydrocyclone separation performance since an increase in pressure drop increases all velocities throughout the hydrocyclone. Therefore, an increase in pressure drop causes a decrease in the cut size.

Table 1. Experimental results.

Test	Pressure		Feed	Ove	er flow	Und	er flow	d ₅₀	R _f
No.	Drop	% by	(gai/min)	% by	(gal/min)	% by	(gal/min)	- (μm)	
	Δ p (psi)	vol.		vol.		vol.			
1	20	1	8.98	0.096	5.38	2.548	3.60	-	0.40
11	30	1	10.89	0.133	6.68	3.559	4.21	-	0.38
Ш	35	1	11.74	0.107	7.35	3.362	4.39	-	0.37
IV	20	2	8.64	0.207	5.08	5.088	3.56	-	0.41
V	30	2	10.53	0.218	6.54	6.321	3.99	-	0.38
VII	35	2	11.81	0.216	7.42	3.632	4.39	-	0.37
VII	20	5	8.47	3.030	4.91	11.340	3.56	40	0.42
VIII	30	5	11.28	3.415	6.93	14.163	4.35	11	0.38
IX	35	5	11.56	0.978	7.21	8.200	4.35	2	0.37
X*	30	0.20	9.62	3.74	3.15	3.95	6.47	-	0.67
XI*	30	0.37	9.32	0.78	1.45	3.92	7.87	-	0.84
XII*	35	1	10.01	0.22	3.62	0.87	6.39	-	0.64
XIII*	35	2	10.61	0.38	3.95	1.43	6.66		0.63

^{*} Hydrocyclone with vortex finder attachment (Fin).



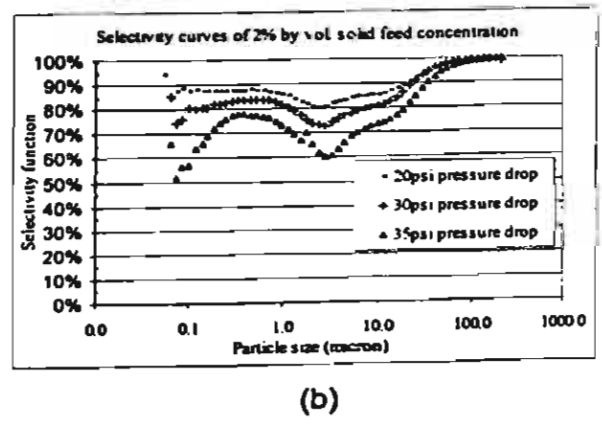


Figure 8. Selectivity curves of the feed solid concentration: a) 1% and b) 2% by volume for 20, 30 and 35psi.

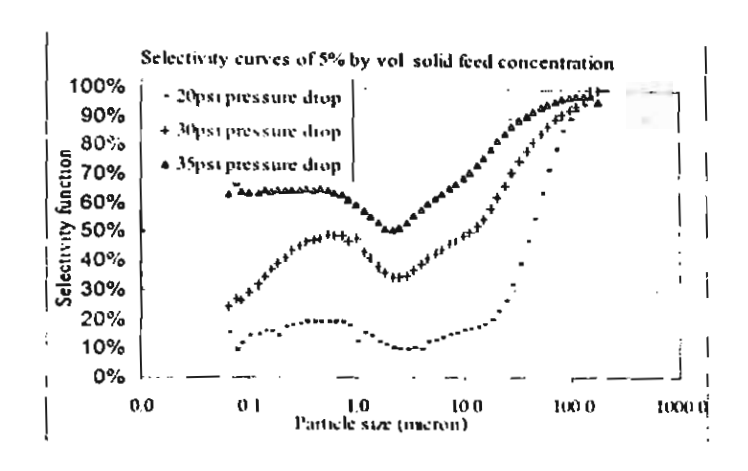


Figure 9. Selectivity curves of the feed solid concentration of 5% by volume for 20, 30 and 35psi.

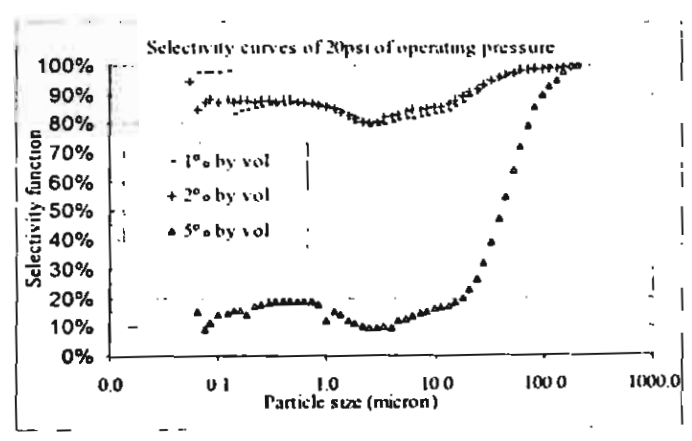


Figure 10. Selectivity curves of the operating pressure of 20 psi for 1, 2 and 5% by volume of solid in feed.

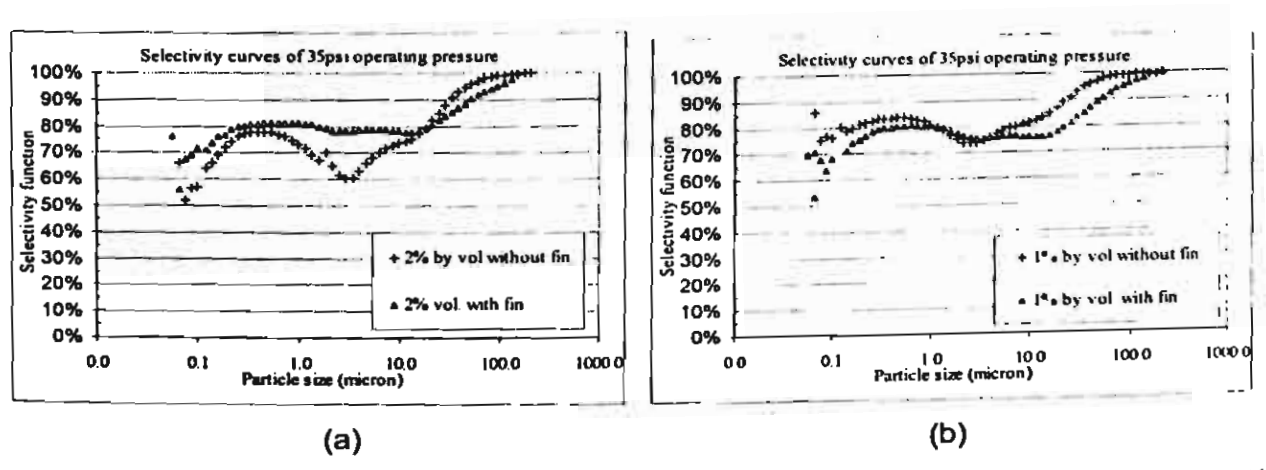


Figure 11. Selectivity curves of the operating pressure of 35 psi for: a) 1% and b) 2% by volume of solid in feed for the hydrocyclone operated with and without fin.

The pressure drop used in practice usually depends on economic considerations. Operating at high-pressure means less units are required to treat a given flow. Lower capital costs, finer cut sizes and sharper separations can be obtained. These benefits must be offset against drawbacks including higher pumping cost and increased abrasion. Furthermore, the increase in feed flow-rate and the decrease in cut size tend to decline above a certain pressure drop. This is thought to be due to resistance effects within the hydrocyclone (Bradley, 1965). More details about the effects of the feed properties and the operational conditions on the separation performance can be found in Kraipech (2002).

The cut size of the 50-mm hydrocyclone unit treating CaCO₃ slurry also strongly depends on the feed concentration. It also appeared that the angle of the underflow discharge at an operating pressure of 35 psi was the smallest angle compared to those at 20 and 30 psi. The discharge of the separator contains the information which could possibly be used for better operational control, assuming that two distinct operational states of the hydrocyclone exist, which are the following: spray and roping. The states differ by the discharge profile from the apex. Roping tends to form a rope-like discharge, while spray resembles an umbrella. Concha et al. (1996) points out that the best separation occurs near the formation of rope discharge. Similarly, Neesse et al. (2003) states on a broader note that a hydrocyclone achieves the best separation at a transitional discharge phase between roping and spraying. Therefore, with the calculation of the angle, determination of the operating performance of the hydrocyclone can be predicted. It is of interest to establish a procedure for improving the operation of hydrocyclones based on computational simulations.

A characteristic dip or fish-hook effect was observed in all experiments. It started to occur at particle sizes of approximately 2 microns. The analysis of this phenomenon is described in Kraipech (2002).

The separation performance of the hydrocyclone with the fin attachment was investigated for the feed concentration of 0.20, 0.37, 1 and 2% by volume. The results of the dilute feed (0.20 and 0.37% by volume) showed that the concentration of the underflow stream was ten to twenty times higher than that of the feed, but the selectivity curve showed low sharpness of separation and the cut size could not obtained. The fin attachment causes an

increase in the throughput ratio. The results of the 1 and 2% by volume of the feed concentration showed very poor results as shown in Figure 11. The operation with 5% by volume of the feed slurry was also examined, and it was found that there was no overflow stream. This is due to the effect of the fin attachment forcing the flow swirling down to the apex tip and the high viscosity of the high concentration feed causing higher drag force, which reduces the effect of the centrifugal force. It can be summarised that the fin-type vortex finder attachment could not increase the sharpness of separation but it could help in the thickening process for a dilute feed system.

6. Conclusion

The results demonstrate that the air core is related to the type of underflow discharge and is a function of the pressure drop, which has an effect on the separation performance of the hydrocyclone. It can be seen that the separation performance does not depend only on the geometry and operating conditions, but also on slurry concentration. The results of this study are useful since they offer an ideal for improving hydrocyclone design and will assist in the validation of computational fluid dynamics (CFD) simulations.

7. References

Bloor, M. I. And Ingham, D. B. "Theoretical investigation of the flow in a conical", Transactions of the Institution of Chemical Engineers, Vol. 51, pp. 36-41, 1973.

Bloor, M. I. And Ingham, D. B. "Turbulent spin in a hydrocyclone", Transactions of the Institution of Chemical Engineers, Vol. 53, pp. 1-6, 1975.

Bloor, M. I. And Ingham, D. B. "The flow in industrial cyclones", J. Fluid Mech, Vol. 178, pp. 507-519, 1987.

Bond, J., Cullivan, J. C., Climpson, N., Dyakowski, T., Faulks, I., Jia, X., Kostuch, J. A., Payton, D., Wang, M., Wang, S. J., West, R. M. and Williams, R. M. "Industrial monitoring of hydrocyclone operation using Electrical Resistance Tomography", 1st World Congress on Industrial Process Tomography Buxton, Greater Manchester, April 14-17, 1999.

Bradley, D. "The Hydrocyclone", Oxford: Pergamon Press, 1965.

Concha, F., Barientos, A., Munoz, L., Bustamante, O. and Castro, O. "A phenomenological model of a hydrocyclone", in Claxton, D., Svarovsky, L. and Thew, M.

(Eds), *Hydrocyclones '96*, London: Mechanical Engineering Publications Limited, pp. 63-82,1996.

١

Hsieh, K. T. and Rajamani, R. K. "Mathematical model of hydrocyclone based on physics of fluid flow", AIChE Journal, Vol. 37. No. 5, pp. 735-745,1991.

Kelsall, D. F. "A study of the motion of solid particles in a hydraulic cyclone", Transactions of the Institution of Chemical Engineers, Vol. 30, pp. 87-108, 1952.

Kraipech, W. "Studying performance of industrial hydrocyclones", Ph.D. Thesis, UMIST, UK, 2002.

Neesse, T., Schneider, M., Dueck, J., Golyk, V., Buntenbach, S., Tiefel, H. "Hydrocyclone operation at the transition point rope/spray discharge". In: Hydrocyclones 2004 in South Africa, 2003.

Pericleous, K. A. and Rhodes, N. "The hydrocyclone classifier: A numerical approach", International Journal of Mineral Processing, Vol. 17, pp. 23-43, 1986.

Svarovsky, L. "A short course in cyclones", Manual to Course at the Dow Chemical Co. in Freeport/Texas, January 10-11, 1994.

Exploitation (or Output) of the project

1. Two Publications in International Journals

1.1. Title: An investigation of the effect of the particle-fluid and particle-particle

interactions on the flow within a hydrocyclone

Authors: W. Kraipech, A. Nowakowski, T. Dyakowski and

A. Suksangpanomrung

Journal: Chemical Engineering Journal xxx (2005) xxx-xxx

Impact No.: 0.677

Paper: See Appendix A

1.2. Title: Numerical prediction of outlet velocity patterns in solid-liquid

separators

Authors: Michael J. Doby, Wanwilai Kraipech and Andrzej F. Nowakowski

Journal: Chemical Engineering Journal xxx (2005) xxx-xxx

Impact No.: 0.677

Paper: See Appendix B

2. Three Presentations in International Conferences

2.1. Title: An investigation of the effect of the particle-fluid and particle-particle

interactions on the flow within a hydrocyclone

Authors: W. Kraipech, A. Nowakowski, T. Dyakowski and

A. Suksangpanomrung

Conference: Solid-Liquid Separation Systems IV Conference organized by

American Filtration Society, British Filtration Society and American Institute of Chemical Engineers (AIChE) at Pucon, Chile, 14-19

December 2003.

Paper: See Appendix A

2.2. Title: Numerical prediction of outlet velocity patterns in solid-liquid

separators

Authors: Michael J. Doby, Wanwilai Kraipech and Andrzej F. Nowakowski

Conference: Solid-Liquid Separation Systems IV Conference organized by

American Filtration Society, British Filtration Society and American

Institute of Chemical Engineers (AlChE) at Pucon, Chile, 14-19

December 2003.

Paper: See Appendix B

2.3. Title: The experimental study of the flow within a transparent hydrocyclone

with a vortex finder attachment

Authors: Wanwilai Kraipech and Andrew F. Nowakowski

Conference: American Filtration and Separations Society Annual Conference 2005

at Atlanta, GA, 10-13 April 2005.

Paper: See Appendix C

3. One Preparing Manuscript for Future publication for International Journals

3.1. Title The simulation of the flow within a hydrocyclone operating with an air

core and with an inserted metal-rod.

Authors: W. Kraipech, A. Nowakowski, T. Dyakowski and

A. Suksangpanomrung

Journal: International Journal of Mineral Processing

Impact No.: 0.539

Appendix A

Title: An investigation of the effect of the particle-fluid and particle-particle interactions

on the flow within a hydrocyclone

Authors: W. Kraipech, A. Nowakowski, T. Dyakowski and A. Suksangpanomrung

Journal: Chemical Engineering Journal xxx (2005) xxx-xxx



Chemical Engineering Journal xxx (2005) xxx-xxx



An investigation of the effect of the particle—fluid and particle—particle interactions on the flow within a hydrocyclone

W. Kraipech^{a,*}, A. Nowakowski^b, T. Dyakowski^c, A. Suksangpanomrung^d

Department of Chemical Engineering, Srinakarinwirot University, Ongkharuk, Nakorn-Nayok 26120, Thailand
 Department of Mechanical Engineering, University of Sheffield, Mappin Street, Sheffield S13JD, UK
 Department of Chemical Engineering, UMIST, PO Box 88, Manchester M6010D, UK

Department of Mechanical Engineering, Academic Division, Chulachomklao Royal Military Academy, Nakorn-Nayok 26001, Thailand

Unitract

The effect of the particle-fluid and particle-particle interactions of the flow within a hydrocyclone is investigated. These were studied by applying the time scale analysis. It is shown that the particle-particle interactions, due to the lubrication and collision mechanisms, only play an important role in the vicinity of a hydrocyclone wall, and near the air core. In the remaining region, particle-fluid interactions are dominating. These play a vital role on the separation efficiency as illustrated by the significance of the wakes generated behind larger particles on dragging finer particles.

02005 Elsevier B.V. All rights reserved.

Repeards: Particle-fluid interaction; Hydrocyclone; Time-scale analysis

1. Introduction

A hydrocyclone is a type of separation equipment used for solid-liquid and liquid-liquid systems. It is used to separate dispersed particles from a continuous fluid as the effect of a swirl flow, and has been used in many mineral processing and mining industries.

In modelling the hydrocyclone performance, the influence of the particles on the flow is significant, particularly in the dense slurry flow, when the exchange of momentum from the particle—fluid, particle—particle and particle—wall interactions affect the velocity of the fluid. This may cause inefficiency in separation performance. The previous works presented by Bloor and Ingham [3–5], Pericleous and Rhodes [16], Pericleous [15] and Hsieh and Rajamani [10] discounted the effects of the presence of particles on a slurry velocity field by assuming that the flow is diluted (solids concentrate less than 5%), and the particle—fluid interaction for a single particle moving through a liquid without the presence of other particles was applied. However, when solids con-

centrate exceeds 5%, the presence of particles changes the velocity stresses and results in the generation of extra inertial stresses. The constitutive formulae, describing complex particle-fluid and particle-particle interactions are required. Generally, these formulae are very complicated as they take into account the spatial and temporal non-uniformities in the particle distributions as well as the acceleration of relative velocity.

There are two main approaches that can be applied to modelling multi-phase systems. They are a multi-fluid model and particle tracking method. The choice of one particular approach is determined by the character of the predominant interaction between the phases. The purpose of this study is to investigate the method for determining the predominant particle interaction of the flow within a hydrocyclone. From this knowledge, the proper method for modelling particle flow in this separator can be chosen.

In this paper, the equation of motion of a single particle in a fluid, neglecting the presence of other particles, is presented. The influence of neighbouring particles is described. The particle-fluid and particle-particle interactions are analysed using the concept of a time scale analysis introduced by Roco [20]. Here a case study is presented, based on the

Corresponding author. Tel.: +66 6 999 8908; fax: +66 37 322 608.

B-mail address: wanwilai@swu.ac.th (W. Kraipech).

results published by Rajamani and Milin [17] for a 75 mm hydrocyclone. On this basis, the zones of the predominant interaction mechanism can be defined and in turn, a proper choice of a specific approach for modelling the flow within hydrocyclone can be made. As a result, the complexity of the constitutive formulae describing these interactions might be significantly reduced.

2. Particle-particle interaction related to hydrocyclone performance

In general, the hydrocyclone has been assumed to be operating at a steady state where the classical fluid dynamics can be applied. Stokes' law is generally assumed to be valid in order to develop models because it simplifies the mathematical formulation. Brownian movement, entrance effects on fluid, particle interactions, spinning of particles, curl of the fluid, wall interaction and the effect of turbulent fluctuations, are normally ignored or neglected [22]. The equations describing the separation function (see [8]), are based on an assumption that the particle settling velocity is not affected by the presence of other particles, and that it is a monotonic function of the particle size. In such a case it seems reasonable to assume that the separation process is linear and is a monotonic function of particle diameter. In fact, as the particles move to the wall their concentration increases and the interactions between them start to manifest through the interstitial fluid by secondary currents and pressure field changes. These particle interaction mechanisms cannot be neglected. Recently, Kumar et al. [13] measured the settling velocities for particles in a poly-dispersed mixture. It is obvious that Stokes' law cannot be applied in a study where the particle interactions are considered. Their results show that the motion of large particles is influenced only by the total volume fraction of particles within the system. Therefore, the settling velocity of large particles can be described by the Richardson-Zaki equation [18]. On the other hand, the smaller particles move at almost identical velocities to the larger particles. These small particles appear to be dragged with the larger ones. The settling velocities of small particles are even larger than the corresponding Stokes velocities or those predicted by the existing theories [2] or correlations.

Taneda's [24] experimental results showed that the permanent vortex-ring behind a sphere begins to form in the rear of a sphere when the critical particle Reynolds number, $Re_p = 24$. The size of the vortex-ring increases for higher Reynolds numbers and the wake behind a sphere begins to oscillate at the rear of the permanent vortex-ring when the Reynolds number is about 130. The latest experimental data of Yang et al. [27] and numerical simulations of Tang et al. [25] show how the dispersion of particles in a wake is organised for small Stokes number particles. Particles with Stokes number less than 1 are able to respond to the small-scale flow pattern and therefore become essentially flow-tracers. The trajecto-

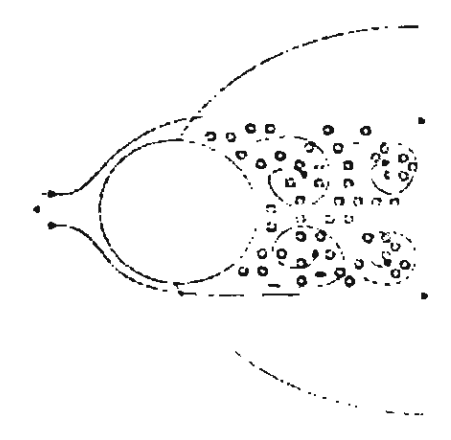


Fig. 1. Dragged mechanism of fine particles by large particle.

ries of these particles distribute themselves throughout the large-scale vortex cores. Conversely particles with a Stokes number much greater than 1 are little affected by the fluid fluctuations at any scale and therefore simply move in the direction of their initial trajectories with only slight deviation.

The ratio between the centrifugal acceleration, w^2/r , and the gravitational acceleration, g, varies along the hydrocyclone radius. The tangential velocity reaches its peak near the hydrocyclone axis. According to Cilliers [6], for a 10 mm

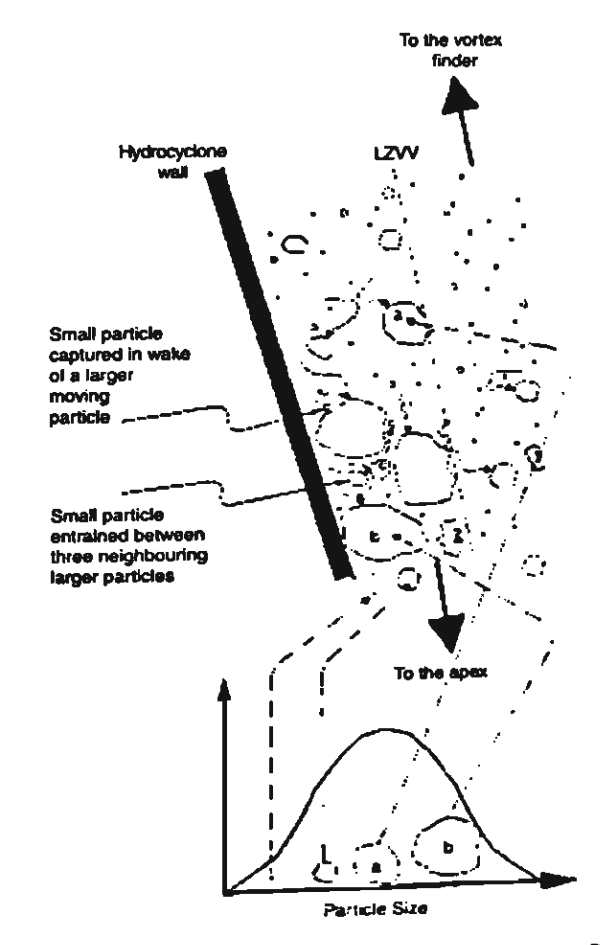


Fig. 2. Mechanisms that describe the fish-hook phenomenon (Roldan-Villasana [21]).

diameter hydrocyclone, the ratio between the centrifugal and gravitational acceleration is around 60,000 and the particle residence time is in the order of milliseconds. These are extreme conditions in relation to the gravitational buoyancy-driven separation of the dispersed phase from the continuous phase.

Therefore, interactions similar to those predicted by Yang et al. [27], and caused by the presence of the vortex-ring behind particles, seems to be worthy of consideration in terms of hydrocyclone performance. These can provide an additional mechanism for finer particles reporting to the underflow in the wake behind the larger particles (see Fig. 1). Such a mechanism may explain the shape of the selectivity curve, and the fact that the bypass value is higher than the water recovery to the underflow. This selectivity curve does not have a sigmoidal shape, but exhibits a dip in regions of finer particle size. This dip is known as the fish-hook effect. The methods of modelling the fish-hook effect of the flow within hydrocyclones, based on this mechanism, were investigated by Kraipech et al. [12].

The hydrodynamic behaviour of hydrocyclones treating concentrated slurries has yet to be fully understood and no accurate theory exists to simulate the phenomena occurring within hydrocyclones. Therefore, the other mechanisms explaining the fish-hook effect proposed by previous researchers such as Roldan-Villasana et al. [22] and Frachon and Cilliers [9], who introduced the idea of an influence from the turbulent dispersion on the motion of fine particles, could

be possible and should not be dismissed. Fig. 2 illustrates the possible mechanisms that describe the fish-hook phenomenon.

3. Equation of particle motion

The equation of motion of a spherical particle in a fluid, neglecting the interactions with other particles can be written as [1]:

$$m_{\rm p} \frac{\mathrm{d}u_{\rm p}}{\mathrm{d}t} = m_{\rm p} \left(1 - \frac{\rho}{\rho_{\rm p}} \right) \mathbf{g} + \mathbf{F}_{\rm D} + \mathbf{F}_{\rm App} + \mathbf{F}_{\rm Bas} + \mathbf{F}_{\rm LS}$$

$$+ \mathbf{F}_{\rm LM} + \mathbf{F}_{\rm PG} \tag{1}$$

where m_p is the mass of the particle, u_p the instantaneous velocity of the particle and g the body acceleration. ρ and ρ_p are the densities of fluid and solid particles, respectively.

The term on the left-hand side of Eq. (1) describes the particle inertia, and the terms on the right-hand side are the forces caused by the particle—fluid interactions as explained in Table 1. When a particle's motion is affected by a neighbouring particle the other forces have to be altered as shown in Table 2.

There are two main causes for lateral lift force on a particle: one is due to the rotation of a particle moving in a fluid, and another is due to the shear of fluid itself, that is, the shear flow induces the lateral lift force even if the rotation of the

Table 1
Forces caused by particle-fluid interactions of a particle flow in a turbulent fluid

Forces	Sources of forces	Equations		
Steady-state drag force, F _D	The force acts on a particle in order to move the particle through a fluid with a uniform pressure and velocity field when there is no acceleration of the relative velocity between the particle and the conveying fluid	$\mathbf{F}_{D} = \frac{1}{2} \rho C_{D} \frac{\mathbf{x} d^{2}}{4} \mathbf{u} - \mathbf{u}_{p} (\mathbf{u} - \mathbf{u}_{p})$	(4)	d is the particle diameter, $(\mathbf{u} - \mathbf{u}_p)$ the relative velocity between fluid and particle and C_D the drag coefficient
Added mass force, F _{App}	The force of the particle on the fluid due to the acceleration of the relative velocity. When a particle is accelerated through the fluid, there is a corresponding acceleration of the fluid, which is at the expense of work done by the particle. This additional work causes the added mass	$F_{App} = \frac{\rho V_p}{2} \left(\frac{du}{dt} - \frac{du_p}{dt} \right)$	(5)	V_p is the particle volume and $\left(\frac{d\mathbf{u}}{dt} - \frac{d\mathbf{u}_p}{dt}\right)$ is the relative acceleration of the fluid with respect to the particle acceleration
Basset force, FBas	force, which is required to accelerate the surrounding fluid The force due to the temporal delay in the boundary layer around the particle development as the relative velocity changes with time. This force takes into account the viscous effects due	$F_{Bas} = \frac{3}{2}d^2\sqrt{\pi\rho\mu}\int_{t_0}^{t} \frac{(du/dt)-(du_0/dt)}{\sqrt{t-t'}}dt'$	(6)	
Saffman lift force, FLS	to the acceleration of the relative velocity The force produced by the pressure distribution developed on a particle due to the rotation	$F_{LS} = 1.615d^2(\mu\rho\dot{\gamma})^{1/2}(u - u_p)$	(7)	$\dot{\gamma}$ is the rate of fluid deformation
Magnus lift forces, F_{LM}	induced by a fluid velocity gradient The force due to the rotation of the particle. This force is caused by a pressure difference between both sides of the particle resulting	$\mathbf{F}_{LM} = \frac{1}{2}\rho(\mathbf{u} - \mathbf{u}_{p})^2 C_{L} \frac{\pi d^2}{4}$	(8)	C _L is the lift force coefficient
house gradient force, Fro	from the velocity difference due to the rotation The force due to the pressure gradient in the fluid surrounding the particle	$\mathbf{F}_{PG} = -V_p \nabla p$	(9)	

Table 2
The effect of neighbouring particles on the particle motion

Distance between particles, L	Flow mechanism	Flow diagram
$\frac{L}{d} > 10$	No interaction between particles	O← L → O
½ ≈ 2	Vortex shedding	₹ <u>€</u> ′, < , < O',
½ ≈ 0.5	Lubrication	⊕ ⊕
± = 0	Collision	⊕ ⊕

Table 3
Time scales for particle interactions in the hydrodynamic range [20]

Type of particle interaction	Time scale, t _m	Comments		
Liquid-solid interaction (drag)	$t_{\rm d} = \frac{4}{3} \frac{sd}{C_{\rm D} u - u_{\rm p} }$	(10)	$C_D = f(Re_p)$, Re_p is the particle Reynolds number	
Lubrication	$t_{lub} = \frac{18}{s} \frac{\lambda}{\dot{\gamma}_{ij}}$	(11)	$\lambda = \frac{1-(\alpha^*)^{0.33}}{(\alpha^*)^{0.33}}$, where $\alpha^* = \frac{\alpha}{\alpha_{max}}$	
Collision	$t_{\rm col} = \frac{45}{s_{\rm Nj}} + \frac{4.5}{s_{\rm Nj}} \ln(\lambda)$	(12)	The first term on the right-hand side corresponds to the particle roughness	

particle is absent. The former is called the Magnus effect and the latter is the Saffman effect, which are additionally described in Table 1. The Saffman lift force is predominantly induced when a solid particle moves in a region with a shear flow of a steep velocity gradient in the surrounding fluid. When the rotation of a particle is given from the beginning of the transport, the Magnus lift force is predominant.

Dense flow is characterised by high collision frequencies between particles, and hence their motion is dominantly influenced by particle—particle collisions. Interactions between the fluid and particles are of minor importance [23]. The models for predicting the collision forces are not discussed here but they can be found in the references of Crowe et al. [7], Tsirkunov and Panfilov [26] and Sommerfeld [23]. Generally speaking, the collision force depends on the properties of the particles such as density and surface roughness, as well as on the magnitude and the direction of the relative velocity.

The lubrication interaction is the particle-particle interaction due to the pressure in a fluid, which is generated by the particles approaching each other. This pressure can be calculated using the lubrication theory, which neglects all inertial forces in a fluid (creeping flow approach). By integrating this pressure distribution along the particle surface, an additional

force, the lubrication force, acting on the particle can be derived [7]. Assuming that the flow is symmetrical about the centre plane between two, this force can be described by the following equation:

$$F_{\rm Lub} = -\frac{3\pi\mu d^2\dot{h}}{8h_0} \tag{2}$$

where h_0 is the distance between the sphere and the symmetric plane, which is perpendicular to the plane, and \dot{h} the rate at which the sphere is approaching the symmetric plane.

4. Time scale analysis

The frequency of an interaction mechanism's occurrence between particles, or between particles and fluid, is inversely proportional to the time required by the particle to respond to the interaction mechanism.

An interaction mechanism "n" that is characterised by the time scale t_n is more frequent and therefore has a larger distribution to the momentum transfer than another interaction mechanism "m" characterised by the time scale t_m , if $t_n < t_m$. This relation is defined as the relative particle interaction

Relative particle interaction number N. ... (20)

Relative particle interaction number, N _{n,m} [20]		
lelative interaction mechanisms	Significant ratio	Relative particle interaction number
Particle-particle lubrication/particle-liquid drag		$N_{d,lub} = \frac{r^2 d^2 \dot{\nu}_{t,l}}{18^2 v \lambda} \tag{13}$
Particle-particle collisions/particle-liquid drag	<u></u>	$N_{\rm d,col} = \frac{r^2 d^2 N_f}{18 r^2} \frac{1}{45 - 4.5 \ln(\lambda)} \tag{14}$
Particle-particle collisions/particle-particle lubrication	fool fluib fool	$N_{lub,col} = \frac{(3\lambda)}{45 + 45 \ln(\lambda)} \tag{15}$

Note: t_d is replaced by its expression for the Stokesian ($Re_p \le 0.1$) in this table.

THE THE PERSON NAMED IN TH

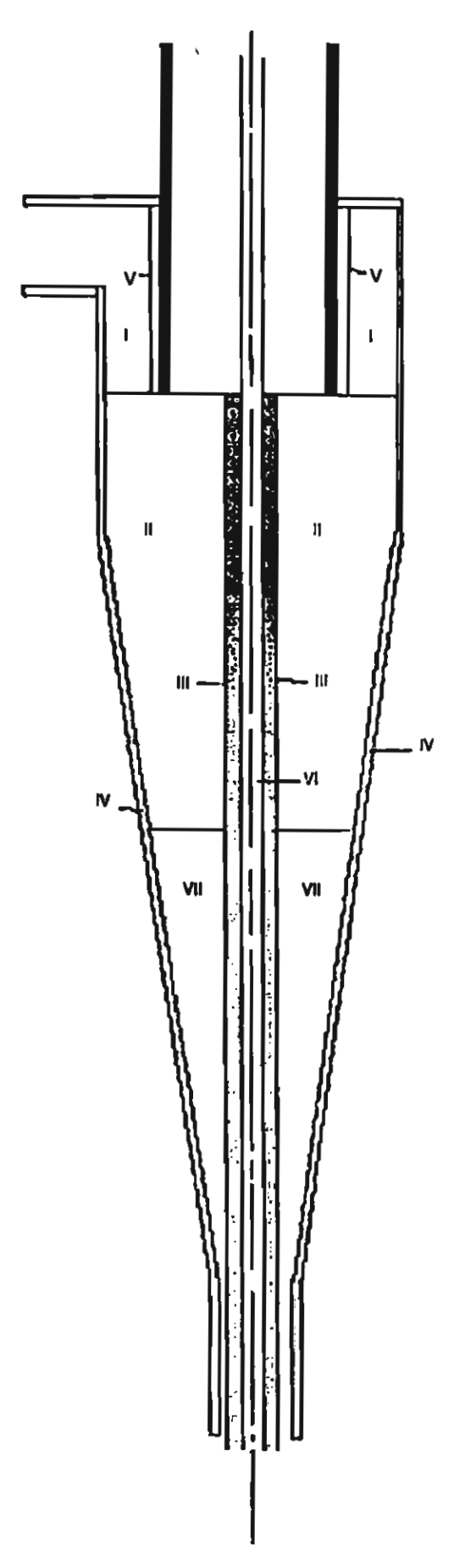


Fig. 3. Zones in the hydrocyclone.

number, $N_{n,m}$.

$$\frac{1/t_m}{1/t_n} = \frac{t_n}{t_m} = N_{n,m} \tag{3}$$

If $N_{n,m} < 1$, the *n*th mechanism is prevalent comparative to the *m*th mechanism.

The time scales responding to liquid-solid (drag), lubrication and collision interactions and the relative particle interaction numbers $N_{n,m}$, are shown in Tables 3 and 4, respectively. They were derived using a similar method as discussed by Roco [19] (see [11]). On the contrary to the drag time scale, the lubrication and collision time scales are dependent on the velocity profile and the solids volume fraction.

5. A case study for calculating the time scales of the flow within a hydrocyclone

In this study, an application of a time scale analysis to identify the predominant interaction is presented for the 75 mm hydrocyclone, based on the experiment and prediction of Rajamani and Milin [17]. The time scales are calculated for seven flow zones within a hydrocyclone, instead of six flow zones, which was carried out in the author's previous work,

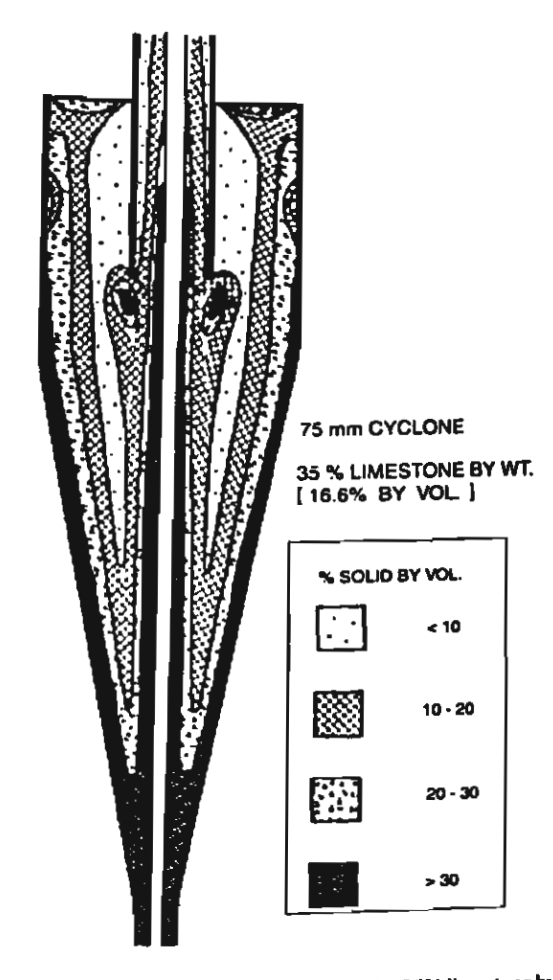


Fig. 4. Predicted volumetric concentration map for 35% limestone by weight (16.6% by volume) in the feed [17].

Table 5
Location of zones

Zone	Location
I	The upper cylindrical part of the hydrocyclone, from the top to the bottom of the vortex finder tube, outside the boundary layer on the outer wall of the vortex finder. Because of the high level of turbulence and secondary flows that originate due to the tangential entrance, the flow is well mixed containing a homogeneous suspension
п	The middle part of the hydrocyclone from the bottom of the vortex finder tube to the middle of the conical section outside the boundary layer on the lateral walls and the boundary layer near the air core
Ш	The area near the air core
ľV	The boundary layer on the lateral walls. The boundary layer starts at the feed and develops its maximum thickness when reaching the level of the bottom of the vortex finder tube
V	The boundary layer at the outer wall of the vortex finder
VI	The air core, which is assumed to have a cylindrical shape
VII	The lower part of the hydrocyclone from the middle to the end of the conical section outside the boundary layer on the lateral walls and the boundary layer near the air core

Table 6
The experimental selectivity values [17]

Particle size (µm)	Percent of solid recovery to underflow
90	100
65	92
45	80
33	52
23	30
16	20
11	16
	11
4	10
3	9
1	7

Kraipech [11]. The locations of each zone are described and shown in Table 5 and Fig. 3.

The feed slurry of the case study is 35% by weight of limestone (16.6% by volume). The liquid phase is water, which has a density of 1000 kg/m^3 and a kinematic viscosity of $10^{-6} \text{ m}^2/\text{s}$. The density of limestone is 2700 kg/m^3 and its volume fraction at maximum packing is 0.7. The particle size is in the range of $1-90 \mu \text{m}$ (Table 6). The volumetric concentration map and tangential velocity profile are shown in Figs. 4 and 5, respectively.

The time scales and their relative particle interaction numbers are the functions of flow data such as the velocity field, particle sizes and the solid concentration, as shown in Tables 3 and 4. Therefore, it is possible to calculate the time scales and their relative particle interaction numbers for a given set of data describing the flow.

Fig. 5. Measured and predicted tangential velocities in a 75 mm hydrocyclone [17].

Table 7
The flow characteristics in each year in the hydrogenologies

Zone	Volume fraction, α	Particle size (µm)	The mean rate of strain tensor, $ \dot{y}_{r\theta} = \frac{r}{2} \left \frac{\partial}{\partial r} \left(\frac{w}{r} \right) \right (s^{-1})$
1	$\alpha < 0.1$; $0.1 < \alpha < 0.2$; $0.2 < \alpha \le 0.3$	1-90	107
4	$\alpha < 0.1$; $0.1 < \alpha < 0.2$; $0.2 < \alpha \le 0.3$	I-90	110
Щ	α>0.3	1-90	570
īV	α>0.3	1-90	179
V	α < 0.1	1-65	19
٧L	_	_	-
¥II	$\alpha < 0.1$; $0.1 < \alpha < 0.2$; $0.2 < \alpha \le 0.3$	1–90	187

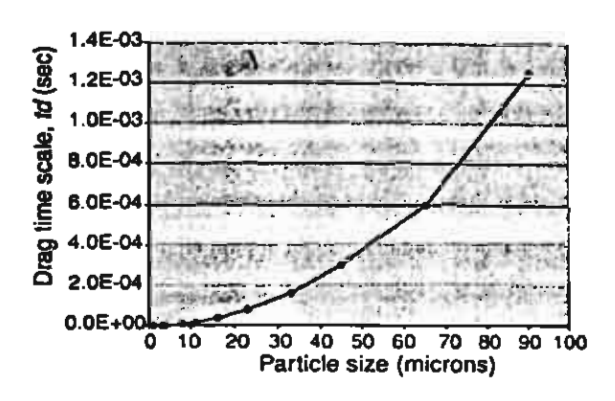


Fig. 6. Drag time scale, t_d , of the limestone particle flow in water (kinematic viscosity of 10^{-6} m²/s) obtained from the experimental results of Rajamani and Milin [17].

Eqs. (10)-(12) are used to calculate the drag, lubrication and collision time scale. The flow around the particle is assumed to be in the Stokes' law region. Therefore, $C_D = \frac{24}{R\epsilon_0}$. The aqueous suspension of limestone is assumed to be a Newtonian fluid for all range of weigh fraction in order to simplify the calculation, even though the suspension shows a non-Newtonian behaviour when its weight fraction is high. The rate of strain tensor can be calculated from the tangential velocity profile, which is presented in Fig. 5. The component $\dot{\gamma}_{r\theta} = \frac{r}{2} \frac{\partial}{\partial r} \left(\frac{w}{r} \right) + \frac{1}{2r} \frac{\partial v}{\partial \theta}$ of the rate of strain tensor is taken into this analysis, instead of $\dot{\gamma}_{r\theta} = \frac{\partial w}{\partial r}$ which is used in Nowakowski et al. [14]. Assuming that the flow is axisymmetrical, the term $\frac{1}{2r}\frac{\partial \nu}{\partial \theta}$ is neglected. The absolute value of the rate of strain tensor can be calculated as $|\dot{\gamma}_{r\theta}| = \frac{r}{2} \left| \frac{\partial}{\partial r} \left(\frac{w}{r} \right) \right|$. The ratio between the inter-particle distance and the particle diameter, λ , is equal to $\frac{1-(\alpha^{\bullet})^{0.33}}{(\alpha^{\bullet})^{0.33}}$, where $\alpha^{*}=\frac{\alpha}{\alpha_{\max}}$. α_{\max} is the solids volume fraction at maximum packing and α the solids volume fraction obtained from the volumetric concentration as shown in Fig. 4. In this figure, the solids concentation distribution is presented in three ranges of volumetric concentration. According to the experimental results, it is assumed that there are no particles equal to or larger than 90 μm in diameter in Zone V (see Fig. 3). The flow characteristics are summarised in Table 7. The drag time scale as a function of the particle diameter is shown in Fig. 6. The time scales

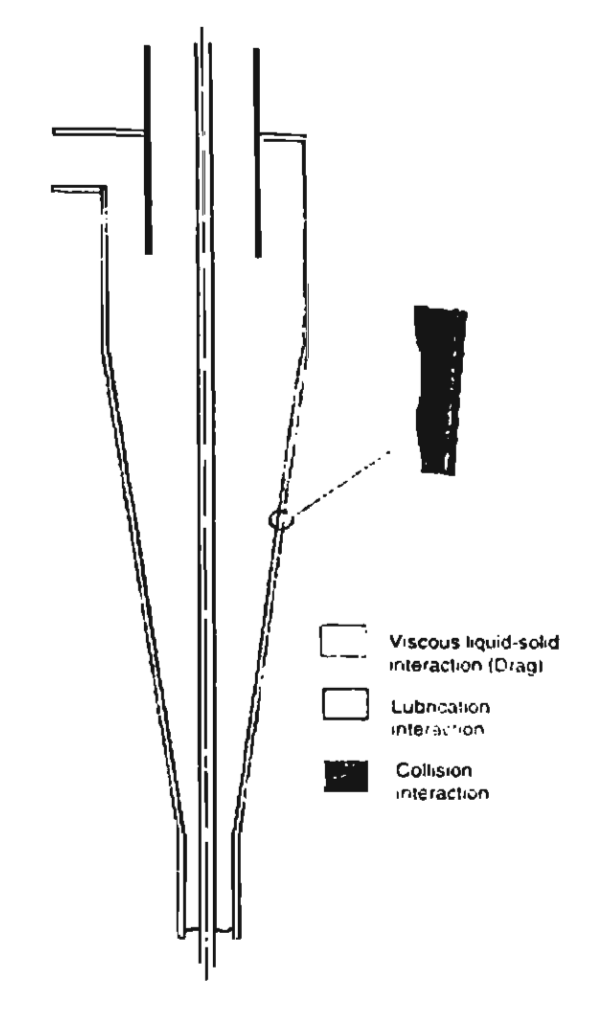


Fig. 7. Main particle interaction mechanisms in the 75 mm hydrocyclone.

for lubrication and collision interactions are presented in Table 8.

Fig. 6 shows that an increase in the particle size leads to an increase in the drag time scale, since a larger particle needs more time to respond to the change in fluid velocity than a smaller one. The lubrication and collision time scales decrease with an increase in the solids volume fraction and the mean rate of strain tensor. This indicates that these two

Librication time scale. t_{lub} , and collision time scales, t_{col}

Zese	Solid concentration (volume fraction)	$t_{\text{lub}} = \frac{18}{s} \frac{\lambda}{\dot{\gamma}_{ij}} \text{ (s)}$	$t_{\rm col} = \frac{45}{i\gamma_{ij}} + \frac{45}{i\gamma_{ij}} \ln(\lambda) (s)$
	$\alpha < 0.1$; $0.1 < \alpha < 0.2$; $0.2 < \alpha \le 0.3$ $\alpha < 0.1$; $0.1 < \alpha < 0.2$; $0.2 < \alpha \le 0.3$	$t_{\text{lub}} > 0.0561$; $0.0561 > t_{\text{lub}} > 0.0319$; $0.0319 > t_{\text{lub}} \ge 0.0201$ $t_{\text{lub}} > 0.0546$; $0.0546 > t_{\text{lub}} > 0.0319$;	$t_{col} > 0.0952; 0.0952 > t_{col} > 0.0864,$ $0.0864 > t_{col} \ge 0.0792$ $t_{col} > 0.0926; 0.0926 > t_{col} > 0.084;$
N N	α > 0.3 α > 0.3	$0.0319 > t_{lub} \ge 0.0201$ $t_{lub} < 0.0037$	$00.0840 > t_{col} \ge 0.0770$ $t_{col} < 0.0149$ $t_{col} < 0.0473$
AI A	α<0.1	t _{hub} < 0.0120 t _{hub} > 0.0316	$t_{\rm col} \ge 0.0536$
_	$\alpha < 0.1$; $0.1 < \alpha < 0.2$; $0.2 < \alpha \le 0.3$	$t_{\text{lub}} > 0.03210.0321 > t_{\text{lub}} > 0.01830.0183$ > $t_{\text{lub}} \ge 0.0115$	$t_{\text{col}} > 0.05450.0545 > t_{\text{col}} > 0.04940.0494$ > $t_{\text{col}} \ge 0.0453$

Table 9
Prevalent interaction mechanism for each flow zone in the hydrocyclone

Zone	Solid concentration condition	Relative particle interaction numbers			Prevalent particle interaction mechanism
		N _{d,hub}	N _{d,col}	N _{lub,col}	
IV	$\alpha \le 0.3$ $\alpha \le 0.3$ $0.3 < \alpha < 0.52$ $\alpha \ge 0.52$ $0.3 < \alpha < 0.64$ $\alpha \ge 0.64$	$N_{d,lub} < 1$ $N_{d,lub} < 1$ $N_{d,lub} < 1$ $N_{d,lub} < 1$ $N_{d,lub} > 1$ $N_{d,lub} < 1$ $N_{d,lub} > 1$	$N_{d,col} < 1$ $N_{d,col} < 1$ $N_{d,col} < 1$ $N_{d,col} < 1$ $N_{d,col} < 1$ $N_{d,col} < 1$ $N_{d,col} < 1$	$N_{\text{lub,col}} < 1$	Liquid-solid interaction (drag) Liquid-solid interaction (drag) Liquid-solid interaction (drag) Lubrication interaction Liquid-solid interaction (drag) Lubrication interaction (drag)
V VI VII	α<0.1 - α≤0.3	$N_{d,lub} < 1$ $-$ $N_{d,lub} < 1$	N _{d,col} < 1 - N _{d,col} < 1	N _{lub,col} < 1	Liquid-solid interaction (drag) - Liquid-solid interaction (drag)

mechanisms are not only dependent on the flow concentration but also on the flow velocity field. The prevalent interaction mechanisms in each flow zone are determined by using the data shown in Fig. 6 and Table 8, and are presented in Table 9 and Fig. 7.

From this analysis, it is found that for the majority of the area within the hydrocyclone, where the solids concentration is less than 30% by volume, the main particle interaction mechanism is the liquid-solid interaction (drag). In the high solids concentration areas, the lateral boundary layer (zone IV) and the area near the air core (zone III), the lubrication and collision interaction mechanisms are prevalent compared with the drag interaction mechanisms. This is in agreement with the work of Nowakowski et al. [14].

6. Conclusion

An application of a qualitative analysis based on a "time scale" concept was presented and discussed to assess the predominant interaction mechanisms within a hydrocyclone. It was found that the liquid-particle interaction (drag) plays an important role in the main body of a hydrocyclone. However, within the regions close to the walls and the air core, both hubrication and collision mechanisms are predominant. This means that the flow pattern within a hydrocyclone should not only be described by interactions between particles and carrying fluid but that the results of solid mechanics should also be included in modelling particle-particle collisions in the vicinity of the hydrocyclone walls. The future work should lead to deriving a simplified model for the particle transport taking into account only the dominating relevant forces in each region. The extension of the analysis to the non-Newtonian behaviour of the high weight fraction of limestone suspentions is also planned.

References

[1] M.K. Akbar, M.A.R. Sharif, R.C. Bradt, Effect of forces on a particle in a straight channel turbulent flow, in: Proceedings of the Fourth International Conference on Multiphase Flow, vol. 53, New Orleans, LA, USA, May 27-June 1, Institution of Chemical Engineers, 2001, Pp. 1-6.

- [2] G.K. Batchelor, Sedimentation in a dilute polydisperse system of interacting sphere. Part 1. General theory, J. Fluid Mech. 119 (1982) 372-408.
- [3] M.I. Bloor, D.B. Ingham, Theoretical investigation of the flow in a conical, Trans. Inst. Chem. Eng. 51 (1973) 36-41.
- [4] M.I. Bloor, D.B. Ingham, Turbulent spin in a hydrocyclone, Trans. Inst. Chem. Eng. 53 (1975) 1-6.
- [5] M.I. Bloor, D.B. Ingham, The flow in industrial cyclones, J. Fluid Mech. 178 (1987) 507-519.
- [6] J.J. Cilliers, Private communication, 2001.
- [7] C.T. Crowe, M. Sommerfeld, Y. Tsuji, Multiphase Flows with Droplets and Particles, CRC Press, USA, 1998.
- [8] B.C. Flintoff, L.R. Plitt, A.A. Turak, Cyclone modelling a review of present technologies, CIM Bull. 80 (1987) 39-50.
- [9] M. Frachon, J.J. Cilliers, A general model for hydrocyclone partition curves, Chem. Eng. J. 73 (1999) 53-59.
- [10] K.T. Hsieh, R.K. Rajamani, Mathematical model of hydrocyclone based on physics of fluid flow, AIChE J. 37 (5) (1991) 735-745.
- [11] W. Kraipech, Studying the performance of mineral hydrocyclones, Ph.D. Thesis, University of Manchester, Institute of Science and Technology, 2002.
- [12] W. Kraipech, W. Chen, F. Parma, T. Dyakowski, Modelling the fish-hook effect of the flow within hydrocyclones, Int. J. Miner. Process. 66 (2002) 49-65.
- [13] S. Kumar, T.W. Pirog, D. Ramkrishna, A new method for estimating hindered creaming/settling velocity of particles in polydisperse systems, Chem. Eng. Sci. 55 (2000) 1893-1904.
- [14] A. Nowakowski, W. Kraipech, T. Dyakowski, R. Williams, The hydrodynamics of a hydrocyclone based on a three-dimensional multicontinuum model, Chem. Eng. J. 80 (2000) 275-282.
- [15] Pericleous, Mathematical simulation of hydrocyclones, Appl. Math. Model. 11 (1987) 242-255.
- [16] K.A. Pericleous, N. Rhodes, The hydrocyclone classifier: a numerical approach, Int. J. Miner. Process. 17 (1986) 23-43.
- [17] R.K. Rajamani, L. Milin, Fluid-flow model of the hydrocyclone for concentrated slurry classification, in: L. Savarovsky, M.T. Thew (Eds.), Hydrocyclone Analysis and Applications, Kluwer Academic Publishers, London, 1992, pp. 59-108.
- [18] J.F. Richardson, W.N. Zaki, Sedimentation and fluidisation, Part 1, Trans. Inst. Chem. Eng. 32 (1954) 35-53.
- [19] M.C. Roco, Dense slurry flow, in: Proceedings of the Advancement in Aerodynamics, Fluid Mechanics and Hydraulics, ASCE, EM & HY Div., 1986, pp. 365-376.
- [20] M.C. Roco, Turbulent flow of incompressible mixtures, in: Encyclopedia of Fluid Mechanics, vol. 10, Gulf Publisher Company, Houston, TX, 1990, pp. 1-68.
- [21] E.J. Roldan-Villasana, Modelling and Simulation of Hydrocyclone Networks for Fine Particle Processing, Ph.D. Thesis, UMIST, Manchester, UK.

- [22] E.J. Roldan-Villasana, R.A. Williams, T. Dyakowski, The origin of the fish-hook effect in hydrocyclone separators, Powder Technol. 77 (1993) 245-250.
- [23] M. Sommerfeld, Validation of a stochastic Lagrangian modelling approach for inter-particle collisions in homogeneous isotropic turbulence, Int. J. Multiphase Flow 27 (2001) 1829–1858.
- [24] S. Taneda, Studies on wake vortices (III): experimental investigation of the wake behind a sphere at low Reynolds numbers, Rep. Res. Inst. Appl. Mech. IV 16 (1956) 99-105.
- [25] L. Tang, F. Wen, Y. Yang, C.T. Crowe, J.N. Chung, T.R. Troutt, Self-organizing particle dispersion mechanism in a plane wake, Phys. Fluids A4 10 (1992) 2244-2251.
- [26] Y.M. Tsirkunov, S.V. Panfilov, Modelling of particle-wall interaction in two-phases flows at moderate and high particle impact velocity, in: Proceedings of the Third International Conference on Multiphase Flow, ICMF 98, Lyon, France, June 8-12, 1998.
- [27] Y. Yang, C.T. Crowe, J.N. Chung, T.R. Troutt, Experiments on particle dispersion in a plane wake, Int. J. Multiphase Flow 26 (2000) 1583-1607.

Appendix B

Title: Numerical prediction of outlet velocity patterns in solid-liquid separators

Authors: Michael J. Doby, Wanwilai Kraipech and Andrzej F. Nowakowski

Journal: Chemical Engineering Journal xxx (2005) xxx-xxx



Chemical Engineering Journal xxx (2005) xxx-xxx



Numerical prediction of outlet velocity patterns in solid-liquid separators

Michael J. Doby a,*, Wanwilai Kraipech b, Andrzej F. Nowakowski a,c

Chemical Engineering Department, UMIST, P.O. Box 88, Manchester M60 10D, UK

b Department of Chemical Engineering, Srinakharinwirot University, Rangsit-Nakhonnayok Rd, Klong 16, Ongharak, Nakhonnayok 26120, Thailand
C Department of Mechanical Engineering, University of Sheffield, Mappin Street, Sheffield S1 3JD, UK

Abstract

Three-dimensional simulations of incompressible fluid flow within hydrocyclone have been performed using the developed numerical technique. A discretization of the physical problem has been done by using a finite element method based on mixed approximation of the velocity and pressure space. The approach offers significant advantages in the solution process of convection dominated internal flows having one inlet and more than one outlet. It deals with the complex geometry of the head entry part of hydrocyclone. The boundary conditions represent forces and are efficiently incorporated into the numerical formulation. Such formulation is very useful since it allows modeling the characteristic velocity profile in the outlet. We investigate the interaction between the swirling flow and velocity profile at the outlet. The studies are carried out for fluids with different properties and can be extended to hydrocyclones with different geometrical configurations.

© 2005 Elsevier B.V. All rights reserved.

Experience Solid-liquid separators; Discharge angle; Hydrocyclone design; Numerical simulation

L Introduction

The discharge of solid-liquid separators contains the information, which could possibly be used for better operational control. The work presented endeavors to establish a procedure for improving operation of hydrocyclones based on computational simulations. The complex nature of the flow in hydrocyclones drastically changes depending on the operating conditions. Since the hydrodynamics of a hydrocyclone are not clearly understood, the design and control of hydrocyclones are primarily based on empirical data. Due to the complicated nature of flow in a hydrocyclone, the models developed to predict the operation and control are still under development. Heiskanen [1] argued that hydrocyclone empirical models available for determining the operational state should be used carefully, because the models did not accurately control or predict the operation of a hydrocyclone. In spite of the shortcomings, the design process of hydrocyclones consists of using empirical models and classification curves, which are based on specific fluid properties. Plitt [2] proposed one of the first models, which used operational parameters and calculated the mean particle size to determine the operational state. Other empirical relationships have been proposed by Lynch and Rao [3] and Nageswararao et al. [4], which compare well with specific experimental data. In spite of the inaccuracies and uncertainties of the empirical models, steps have been made in improving the design of hydrocyclones as demonstrated by Chu and Luo [5]. Due to lack of complex empirical databases for different mixtures and geometries, various methods of controlling the operation of a hydrocyclone are considered.

In order to develop a good control technique, the significant variables to the operation must be determined. The primary operating parameter that can be controlled without changing fluid properties or measuring the solids in the under/overflow is the discharge angle from the apex. Assuming that two distinct operational states of hydrocyclone exist, which are the following: roping and spray. The states differ by the discharge profile from the apex. Roping tends to form a rope-like discharge, while spray resembles an umbrella. Concha et al. [6] points out that the best separa-

B-mail address: m.doby@postgrad.umist.ac.uk (M.J. Doby).

385.8947/\$ — see front matter © 2005 Elsevier B.V. All rights reserved. 10.1016/j.cej.2005.02.014

^{*} Corresponding author.

tion occurs near the formation of rope discharge. Similarly, Neesse et al. [7] states on a broader note that a hydrocyclone achieves the best separation at a transitional discharge phase between roping and spraying. Many researchers have tried to control the operation of a hydrocyclone by using varying non-obtrusive experimental techniques. Van Latum [8] suggested using X-ray imaging during operation to produce density profile cross-sections. Williams [9] used electrical impedance tomography, which produced a cross-section of an operating hydrocyclone. Petersen et al. [10] used image analysis as a controlling mechanism for the hydrocyclone. based on the discharge spray angle. Neesse et al. [11] developed a non-obtrusive manner of controlling the performance based on the angle of the spray discharge using a combination of techniques, which effectively controlled the operation of a hydrocyclone. Van Deventer et al. [12] demonstrated a method of calculating the angle of discharge with the inclusion of gravity. The method that was presented shows that the spray discharge proceeds through three distinct stages, which are the following: initial increasing of angle, flat and the gravitational driven regions [12]. With the calculation of the angle, determination of the operating performance of the hydrocyclone can be predicted as shown by Petersen et al. [10].

Deriving from the analysis of the discharge spray, we proposed a novel approach for controlling the operation of a hydrocyclone. The approach, which is an extension of the computational code of Nowakowski and Dyakowski [13] can be implemented in the design stage to effectively control the operation of the hydrocyclones, or can be applied as a tool to determine the effectiveness of an existing solid—liquid separator by calculating the discharge angle.

2 Problem formulation

In the study, the necessary numerical data are obtained using finite element approximation of incompressible viscous flow. The governing partial differential equations are the continuity equation and the Navier-Stokes equations. The former is a mathematical realization of the incompressibility of the flow, whereas the latter is momentum equation along with a linear constitutive law relating stresses to rates of strains. The primitive variable formulation is expressed in the most general and fundamental "stress-divergence" form [14]. The form is commonly used in finite element methods and rarely in finite difference or volume methods. The advantage of the "stress-divergence" form is that it permits formulation of physically meaningful Neumann boundary conditions via proper accounting of viscous forces.

1. Boundary conditions

Fig. 1 introduces the vertical cross-section of a hydrocydone with the different parts of boundary conditions indi-

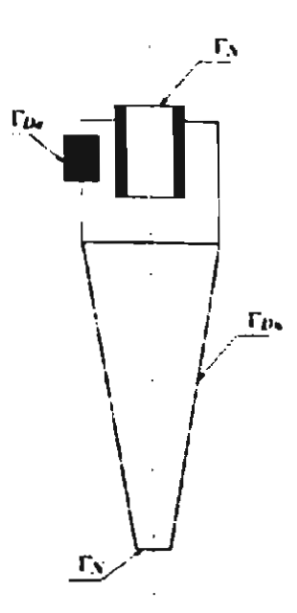


Fig. 1. Boundary conditions of hydrocyclone.

For fluid adjacent to a solid wall, Γ_{Dw} and at the inlet of the hydrocyclone, Γ_{De} the Dirichlet boundary conditions specifying the velocity vectors are imposed. At outflow sections, Γ_{N} Neumann boundary conditions are needed to truncate the computational domain. In the present application, they represent forces and are expressed by:

$$f = \tau n = -pn + 2\nu D(u)n = \hat{f} \tag{1}$$

where τ represents total stress tensor and D(u) deformation tensor equal to the following:

$$\tau = -pI + 2vD(u) \qquad D(u) = 0.5[\nabla u + (\nabla u)^{\mathsf{T}}] \qquad (2)$$

here, n is unit outer vector normal to the boundary, \hat{f} the prescribed body force on the boundary, v denotes the kinematic viscosity of the fluid, u is the velocity vector and pis the scalar pressure. In the performed numerical simulations the "no-stress" boundary conditions were prescribed at the outlets. This is the equivalent of setting f = 0 at the spigot and vortex finder outlet. Such assumption is physically correct, it does not pre-define the parameters of operations, although it may be considered idealistic. Clearly, the stresses exist and can play an important role in the establishment of the velocity profile. The precise value for such stresses is difficult to determine experimentally. Independent of mathematical legitimacy of such boundary conditions, the physics of the matter provides only guidance at best. However, with the lack of the necessary information, the assumption of zero-valued components of forces is natural and advantageous compared to the imposition of specific velocity profile as boundary conditions. The work of Nowakowski and Dyakowski [13] shows that such description has less significant impact on the velocity field. Consequently, the method proposed enables simulations of the characteristic velocity profile at the outlet. In contrast, majority of existing finite volume computational codes for hydrocyclones usually

· 人工人工人工人工人工人工工作。

specify the split ratio or make some assumptions regarding the character of the velocity profile. Such assumptions limit the applicability of simulations performed and consequently the obtained data cannot be used to control the operation of hydrocyclones. Another important advantage of boundary condition, Eq. (1), can be of use when modeling the air core (interface between fluids can be considered as a free boundary).

2.2. Numerical technique

In the finite element method, the flow equations and the associated boundary conditions are solved using the weak form of the governing equations. Then, the continuum problem governed by partial differential equations is reduced by discretization to a system of algebraic equations. The finite element procedure consists of meshing the hydrocyclone geometry into a number of tetrahedral elements. Within each of the elements, the dependent variables (three components of velocity and pressure) are interpolated by suitable polynomials at a set of nodal points. In the present implementation, the adopted element involves a piecewise continuous quadratic approximation of velocities and piecewise constant approximation of pressure. An account of the suitability of different approximation functions and element numerical stability for hydrocyclone simulation is presented in [15]. The comprebensive documentation of the finite element method applied to incompressible fluid mechanics was presented by Gresho and Sani [16].

23. Solution of flow problem

As a solution method, the pressure projection algorithm is implemented by Nowakowski and Dyakowski [13], which is based on some ideas introduced by Haroutunian et al. [17]. The method solves a convection—diffusion equation for velocity, excluding pressure from the momentum equations and updates the pressure while imposing the incompressibility constraint. The velocity field obtained in the first step does not satisfy continuity equation in general. Thus, the velocity field has to be projected onto a divergence-free subspace of the approximation space while updating the pressure. The above described procedure is carried out iteratively using the discrete operators after spatially discretizing the weak form of the Navier—Stokes equations. As a consequence, the boundary conditions, Eq. (1), are consistently incorporated in the algorithm.

14. Calculation of exit profile

The results of the computational fluid dynamics simulation of the hydrocyclone provide the data for calculating the discharge angle. Neesse et al. [7] showed that the farm of the underflow discharge can be used as an indication of the operating state of hydrocyclones. The angle is determined from the velocity components at the spigot

and fluid properties. Lacking the information from the threedimensional flow field, Neesse et al. [7] derived the following equation:

$$\alpha = \arctan\left(\frac{v}{u}\right) \approx \arctan\frac{\rho_{\rm m}(D_u/2u)w^2}{\mu_{\rm m}}$$
 (3)

here, u, v and w are the velocity components in the cylindrical coordinate system of the suspension in the axial (u), radial (v)and tangential direction (w), ρ_m the density of the mixture, $\mu_{\rm m}$ the viscosity of the mixture and $D_{\rm u}$ is the apex diameter. Neesse et al. [7] model assumes boundary conditions that simplify the equations from a three- to two-dimensional problem. For simplification, the flow conditions at the inlet assume an axial symmetrical flow. The assumption of symmetrical flow is not an accurate representation of the flow in the hydrocyclone, as shown by He et al. [18]. The radial velocity was chosen by corresponding a flux to the given flow rate through the inlet. The model assumes that the viscosity of the fluid changes throughout the hydrocyclone, though in the present work the viscosity is set constant. The boundary conditions at the outlet assume that the effluent does not contact the air. Even with the simplifying assumptions for the method proposed by Neesse et al. [7], which will be referred to throughout the paper as the Dueck method, the Dueck method was able to be used to control the operation of the hydrocyclone.

The presented approach, which will be referred throughout the paper as the AFN method, is not limited to axisymmetrical flow. Thus, the AFN method having generated a threedimensional velocity field the angle is calculated directly. Due to the three-dimensional nature of the problem, the complete set of Navier-Stokes equations was solved in a threedimensional framework. The necessary velocity field profiles are obtained using the described finite element approach. An unstructured grid that forms to the shape of a hydrocyclone using tetrahedral elements is generated. One of the reasons that a structured grid was not used may be attributed to a singularity that occurs with the governing equations [19]. Using an unstructured grid helps not only to eliminate the occurrence of singularities but provides full geometrical flexibility. The computer output is in the form of velocity vectors in the u, v and w directions in a Cartesian coordinate system. Using basic trigonometric functions the calculation of the angle is obtained.

Table 1
Fluid properties at different runs with diameter at 22 mm

Number	Reynolds number (Rein)
Run I	220
Run 2	259
Run 3	293
Run 4	338
Run 5	440
Run 6	488
Run 7	505

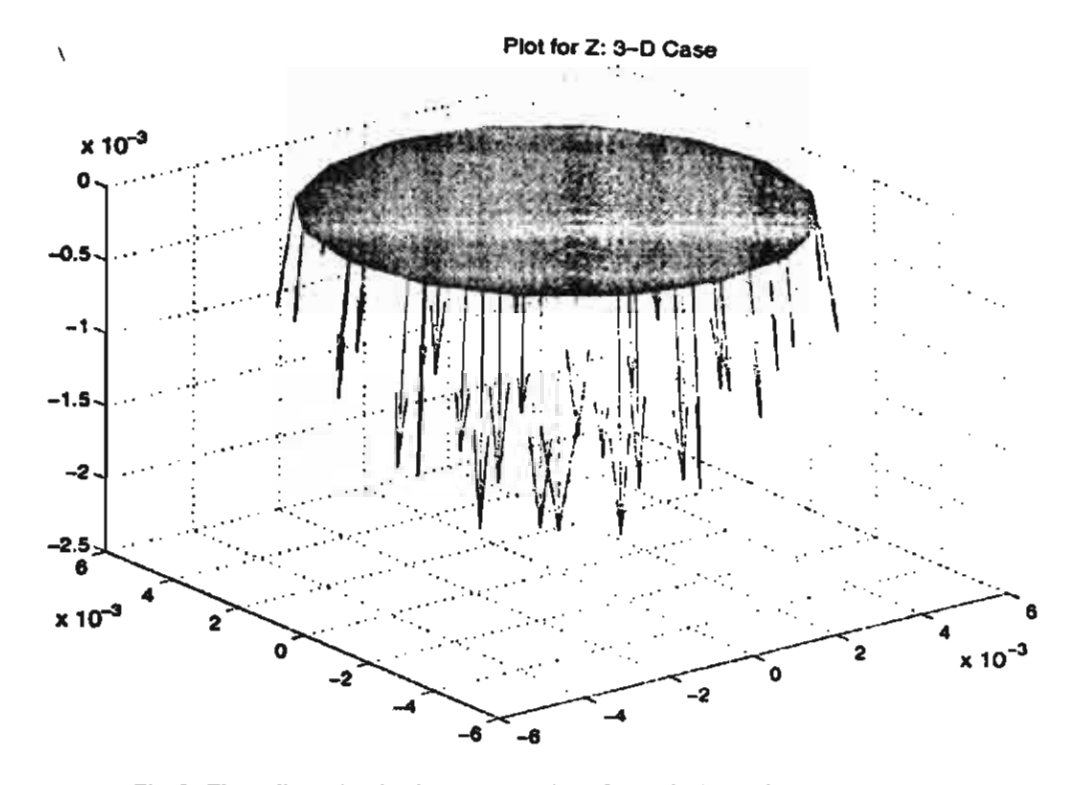


Fig. 2. Three-dimensional quiver cross-section of the velocity profile exiting the apex.

3. Results and discussion

In order to compare the results of the two methods, several formed at different Reynolds numbers at the inlet. The range of viscosities that were chosen kept the flow in the laminar regime. Due properties, the comparison would not introduce any questionable results from using a specific turbulence model. Laminar flow would be equivalent to feeding a viscous slurry in the hydrocyclone. For both methods, the

angle calculations were performed for the same numerically obtained velocity data. In order for equal comparison, the viscosity in the computational domain was assumed to be constant for the Dueck method. Though the neglection of turbulence hydrocyclones is significant even with low inlet Reynolds numbers, a general behavior of the discharge angle can be seen to develop. Table 1 presents the numerical experiment by showing the changes in the Reynolds number at the inlet duct.

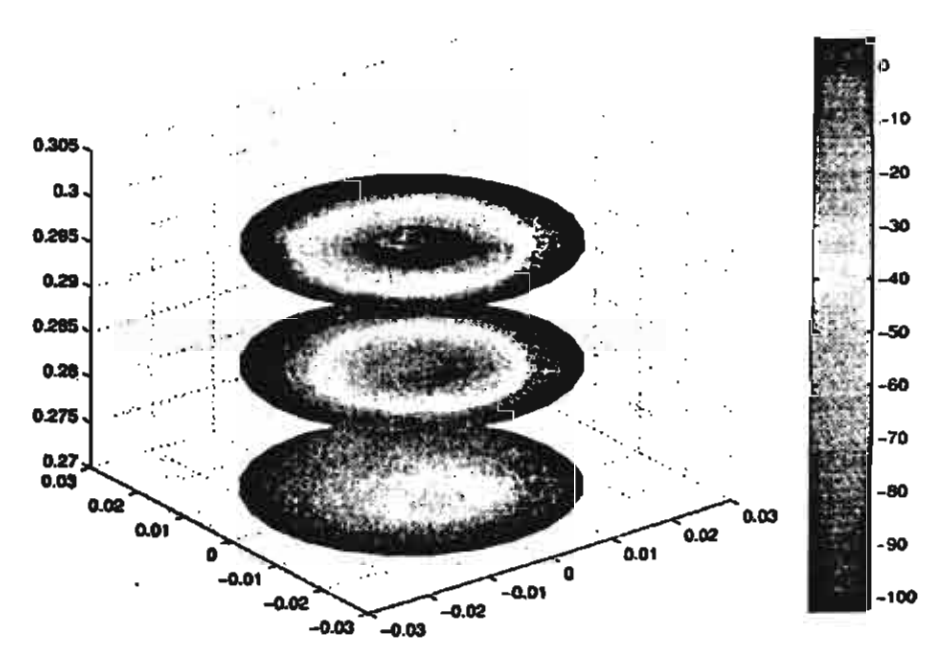


Fig. 3. Cross-section of the pressure profile at the height of 27, 28 and 29 cm.

The Reynolds number was calculated by $Re_{\rm in} = \rho VD/\mu$, where ρ is the density, D the diameter and μ is the dynamic viscosity. The viscosities values decreased after the initial run to compare the change in the form of discharge. Due to the properties of the fluid, the hydrocyclone was operating in the roping region, as shown in Fig. 2.

For clarification, the solid-colored circular contour indicates the location of the exit. As can be seen from Fig. 2, the angle of the exiting fluid is predominately in the downward direction. The roping region can be distinguished from a spray discharge by observing the angle at which the slurry exits along the outer rim of the apex. The roping state tends to show that at the outer edge of the apex the discharge angle is closer to 90 than in spray discharge. However, operating in the experimented region, spray discharge does not occur.

Though in the model we did not take into account the air core, our model reveals the likely mechanism of air core creation. Atmospheric pressure at the center of the apex is the reference point for the pressure field in the hydrocyclone. As noticed in Fig. 3, a pressure reduction occurs toward the center of the hydrocyclone in each of the three different cross-sections. The lowest cross-section indicates that sediment has started to hinder the formation of the low pressure near the center.

As Fig. 3 shows, the bottom of the hydrocyclone has already been semi-plugged with sediment, thus not allowing the low-pressure field to develop at the tip. However, the examination of Fig. 4 reveals that the flow is moving away from the center at the apex.

Processing the data consists of using basic trigonometric functions and using Eq. (3) to calculate the discharge angle. The results of the angle calculated at different viscosities were compared between the AFN and Dueck methods and are listed in Table 2 below.

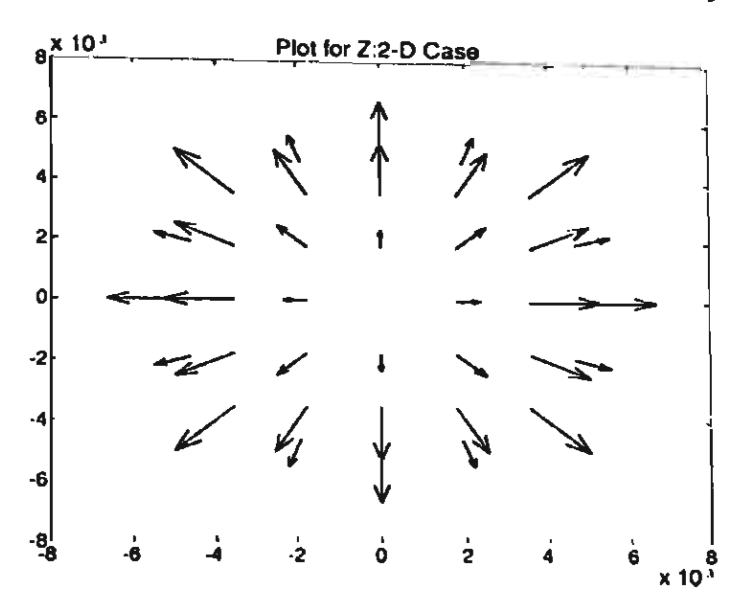


Fig. 4. The two-dimensional velocity profile projected onto the x-y plane cross-section at the apex.

The specific numerical data is not as important as the trend that is shown over the increasing viscosities. The comparison of the results obtained from both methods presents an interesting occurrence. The presented AFN method shows that the angle actually slightly decreases with increasing viscosity. The Dueck method predicts less of a change in the angle than the AFN method at corresponding outlet points. Since the operational state of the hydrocyclone is in roping, the expected angle exiting the spigot should be approximately 90°, which is predicted by both methods at constant viscosity. The possible cause of the inversion trend of the discharge angle at the apex in both methods could be due to the high pressure that occurs at the apex.

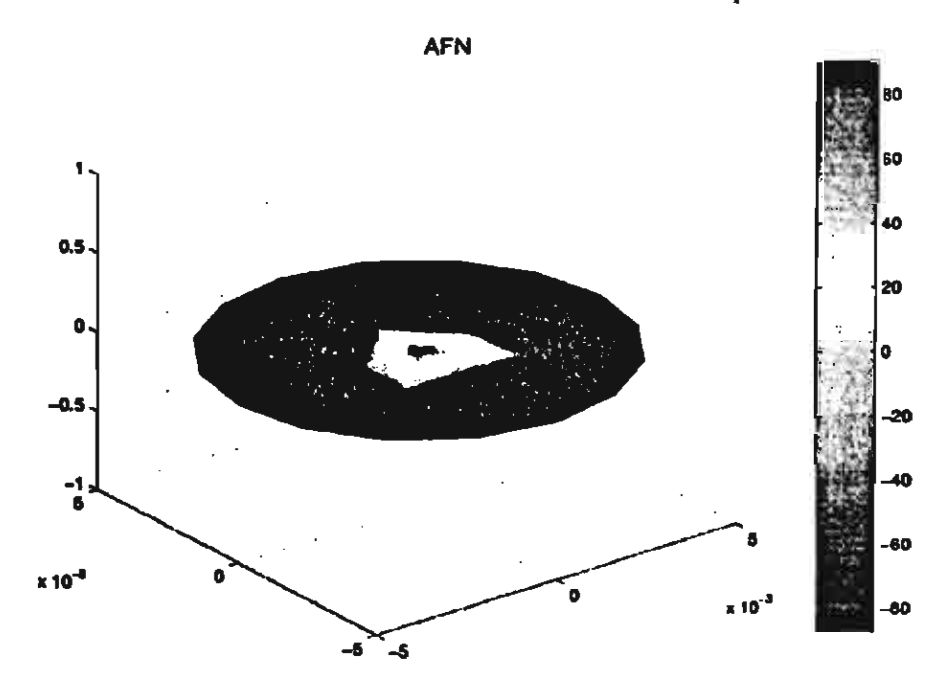


Fig. 5. Cross-section at the apex showing the value of the angle calculated using AFN method [13].

Table 2
Comparison of AFN to the Dueck method at the apex*.b

$\mu = 0.09$		$\mu = 0.15$		μ = 0.2	
AFN	Dueck	AFN	Dueck	AFN	Dueck
90	0	90	0	90	
-87.8287	-89.9999	-86.4223	-89.9999	-85.5935	-89.8999
-85.5519	-89.9986	-83.7236	-89.9985	-82.7164	-88.9985
-80.1776	-89.9 99 9	-77.7033	89.9985	-76.4056	-89.9999
-78.4363	-89.9973	-75.8757	-89.9974	-74.5503	-89.9974

The other runs not presented did not differ excessively.

b µ has units of Pas and density is held constant.

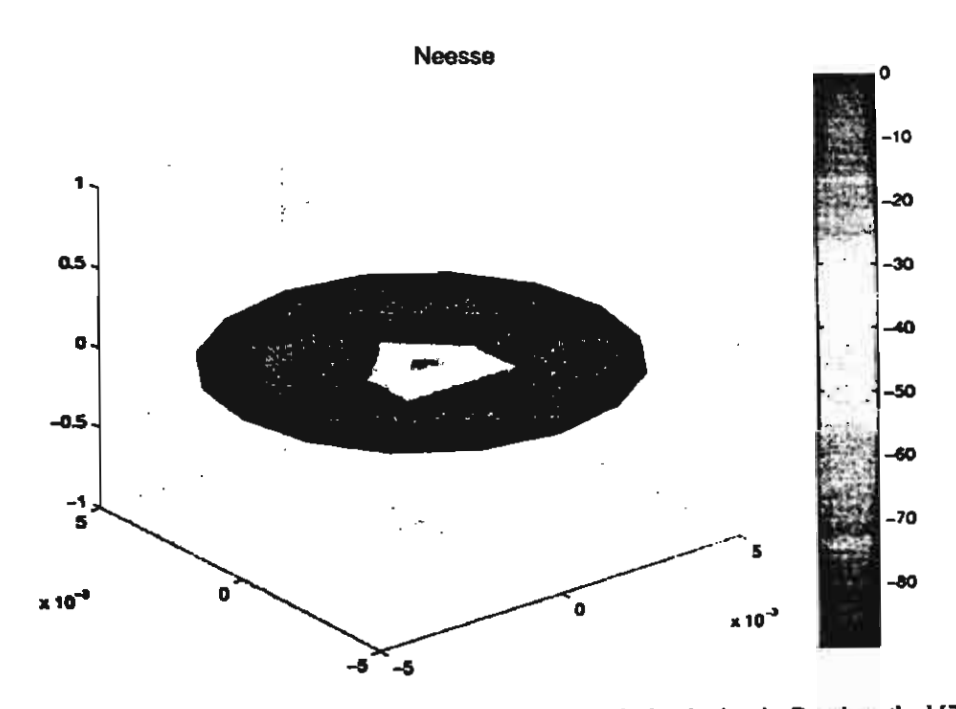


Fig. 6. Cross-section at the apex showing the value of the angle calculated using the Dueck method [7].

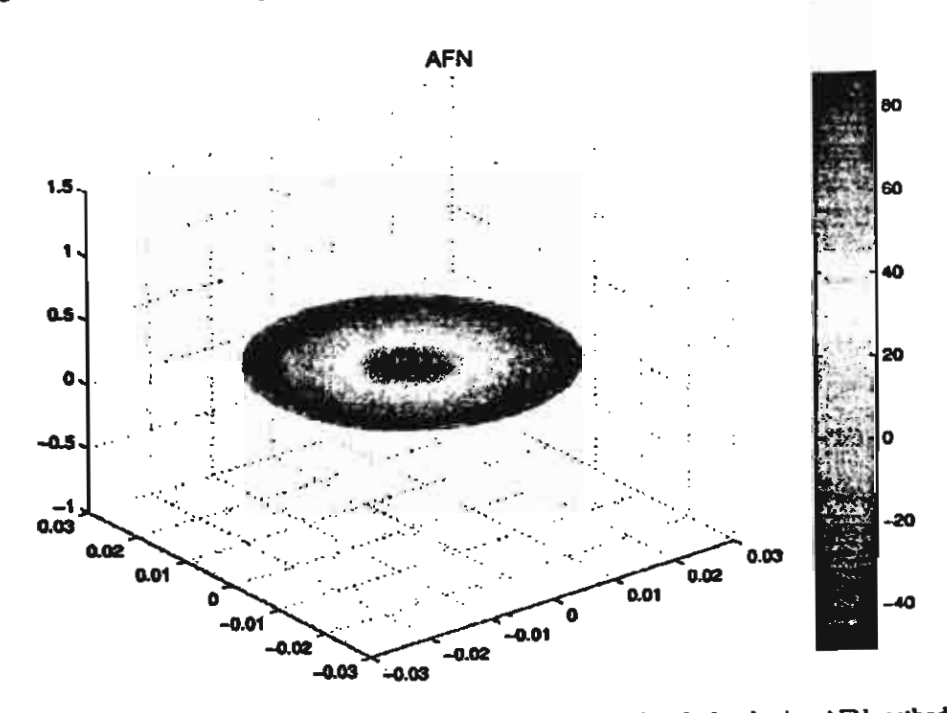


Fig. 7. Cross-section near the vortex finder showing the value of the angle calculated using AFN method [13].

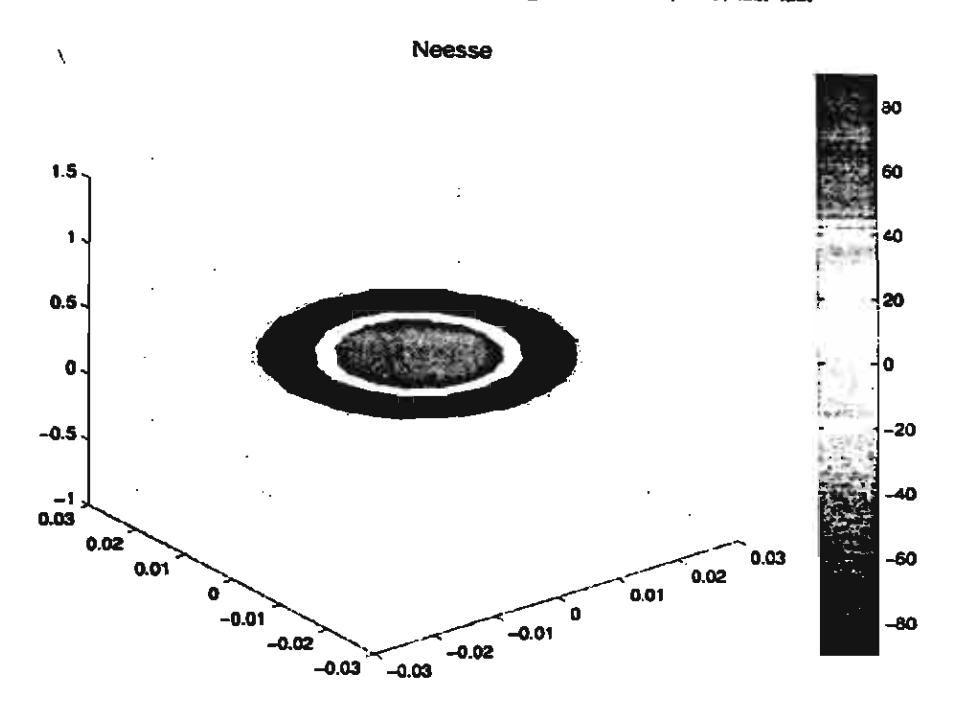


Fig. 8. Cross-section at the apex showing the value of the angle calculated using the Dueck method [11].

A comparison was made between the two different methods at the apex and right below the vortex finder exit, due to the complicated nature of the boundaries. The angles were calculated using both methods at the different cross-sections throughout the hydrocyclone. The following figures show two cross-sections at the apex using the AFN and Dueck methods.

The visual similarity between Figs. 5 and 6 are remarkable. Though at close examination of the legend, the figures illustrate that the gradient of the Dueck angle is steeper than the gradient of the AFN. However, our model predicts that at the center of the apex the actual discharge is in the upward direction, while Dueck's model does not take into account the other velocity vectors beside the tangential direction, w, and axial directions, z. The Dueck method does not predict an angle of discharge at the center of the apex, since the tangential velocity at the center is always zero for the case of axisymmetrical flow. A comparison at the top of the hydrocyclone provides additional insight into both methods.

Again, Figs. 7 and 8 show that the same basic trend of the flow is present. As shown previously, the gradient on the angle is more drastic in the Dueck model than the AFN model. An interesting occurrence happens in both cross-sections at the wall boundary. Both methods illustrate that the stresses from the boundary wall influence the angle. The predicted results qualitatively compared with the experimental results of Fisher and Flack [20], who showed that the shear stresses at the wall caused the velocity to approach or drop below zero.

Conclusion and future work

In conclusion, the study done on the prediction of the anile showed that both approaches tended to show similar an-

gle profiles. Even with the simplification of the equations from three- to two-dimensional, the Dueck method shows a comparable trend to the AFN method. The differences between the two methods is the small variations in the angle calculated with increasing viscosity, which may be due to the increased pressure at the high viscosity. Additionally, experimental verification will need to be done in order to confirm whether or not one method is more accurate than the other, though the Dueck method has already been shown to work for controlling an operational cyclone. However, the trend of both methods at the wall boundary condition coincides with experimental results from Fisher and Flack [20] makes the results look very promising for both methods. The advantage of using the proposed approach is that the velocity profile and split ratio is not explicitly specified initially, thereby allowing the flow field to develop naturally. In the future, the plan is to look at assuming the presence of a non-Newtonian fluid, which allows the viscosity to change through the system. The ultimate goal of the study is to use the analysis of the discharge angle as a tool to assist in hydrocyclone design.

References

- [1] K. Heiskanen, Experimental hydrocyclone roping models, Chem. Eng. J. 80 (2000) 289-293.
- [2] L. Plitt, A mathematical model of the hydrocyclone classifier, Miner. Process. (CIM Bull.) (1976) 114–123.
- [3] A. Lynch, T. Rao, Studies on the operating characteristics of hydrocyclone classifiers, Indian J. Technol. 6 (1968) 106-114.
- [4] Nageswararao, K., Wiseman, D., Napier-Nunn, T., 2003. Two empirical hydrocyclone models revisited. In: Hydrocyclones 2003 in Capetown, South Africa.
- [5] L. Chu, Q. Luo, Hydrocyclone with high sharpness of separation, Filtr. Sep. 31 (1994) 733-736.

- [6] F. Concha, A. Barrientos, J. Montero, R. Sampaio, Air core and roping in hydrocyclones, Int. J. Miner. Process. 44-45 (1996) 743-749.
- [7] T. Neesse, M. Schneider, J. Dueck, V. Golyk, S. Buntenbach, H. Tiefel, Hydrocyclone operation at the transition point rope/spray discharge, Miner. Eng. 17 (5) (2004) 733-737.
- [8] Van Latum, L., 1992. Computed tomographic imaging of a dense media cyclone. In: Applied Research in the Minerals Industry (JKMRC).
- [9] R. Williams, Measurement and modelling of slurry mixing using resistance tomography, in: Proceedings of the XIX International Mineral Processing Congress, Comminution and Simulation and Control, Society for Mining, Metallurgy, and Exploration, Inc. (AIME), 1995.
- [10] K. Petersen, C. Aldrich, J. Van Deventer, C. McInnes, W. Stange, Hydrocyclone underflow monitoring using image processing methods, Miner. Eng. 9 (3) (1996) 301-315.
- [11] T. Neesse, M. Schneider, V. Golyk, H. Tiefel, Measuring the operating state of a hydrocyclone, Miner. Eng. 17 (5) (2004) 697-703.
- [12] J. Van Deventer, D. Feng, K. Petersen, C. Aldrich, Modelling of hydrocyclone performance based on spray profile analysis, Int. J. Miner. Process. 70 (2003) 183-203.

- [13] A. Nowakowski, T. Dyakowski, Investigation of swirling flow structure in hydrocyclones, Trans. IChem. E., Part A, Chem. Eng., Res Des. 81 (A4) (2003) 862-873.
- [14] P. Gresho, Incompressible fluid dynamics: some fundamental issues, Annu. Rev. Fluid Mech. 23 (1991) 413-453.
- [15] Nowakowski, A., Kraipech, W., Dyakowski, T., 2003. Analysis and Simulation of Multifield Problems. Springer, Ch. Performance of some finite elements in numerical simulation of complex incompressible three dimensional flow.
- [16] P. Gresho, R. Sani, Incompressible Flow and the Finite Element Method, Wiley. 1998.
- [17] V. Haroutunian, M. Engelman, I. Hasbani, Segregated finite element algorithms for the numerical solution of large-scale incompressible flow problems, Int. J. Numer. Methods Fluids 17 (1993) 323-348.
- [18] P. He, M. Salcudean, I. Gartshore. A numerical simulation of hydrocyclones, Trans. IChemE 77 (1999) 429-441.
- [19] L. Ma, D. Ingham, X. Wen, A numerical technique for dealing with the axis in simulating the fluid flows in polar cylindrical coordinates, Numer. Methods Laminar Turbulent Flows 10 (1997) 203-214.
- [20] M. Fisher, R. Flack, Velocity distributions in a hydrocyclone separator, Exp. Fluids 32 (2002) 302-312.

Appendix C

Title: The experimental study of the flow within a transparent hydrocyclone with a

vortex finder attachment

Authors: Wanwilai Kraipech and Andrew F. Nowakowski

Presentation: American Filtration and Separations Society Annual Conference 2005 at

Atlanta, GA, 10-13 April 2005.

THE EXPERIMENTAL STUDY OF THE FLOW WITHIN A TRANSPARENT HYDROCYCLONE WITH A VORTEX FINDER ATTACHMENT

Wanwilai Kraipech 1* and Andrew F. Nowakowski²

¹ Department of Chemical Engineering, Srinakharinwirot University Ongkharuk, Nakornnayok 26120, Thailand. Tel.: +66(0)6 999 8908, Fax: 0066(0)37 322 608, E-mail: wanwilai@swu.ac.th

² Department of Mechanical Engineering, University of Sheffield, Mappin Street, Sheffield, S1 3JD, England. Tel.: +44(0)114 222 7812, E-mail: a.f.nowakowski@sheffield.ac.uk

ABSTRACT

The experimental studies of the flow behaviour within 50-mm hydrocyclones with and without a vortex finder attachment (Fin) have been performed. The flow characteristics within both hydrocyclones were observed visually and recorded both photographically and on video as the hydrocyclones are made of a transparent material. The development of the double-helical flow was observed; also the shape and diameter of the air-core have been examined for different values of operating pressure drop. It was found that the air-core is unstable and its size, shape and position are unfixed because of the instability of the gasliquid interface. The results also showed that the air core is related to the shape of the underflow discharge and is a function of the pressure drop. A regular spray discharge from the spigot was observed. The roping discharge was observed when an extension pipe was connected to the underflow outlet. An increase in pressure drop leads to an increase in air-core diameter and the angle of the underflow profile. However, the relationships between these three parameters are non-linear. The knowledge of the size and location of the air-core relative to the operating pressure drop can assist in the validation of computational fluid dynamics (CFD) simulation work.

The separation performance of these two transparent hydrocyclones for a CaCO₃ in water system has been investigated. In this study, the results showed that a fin-type vortex finder attachment could not increase the sharpness of separation but it could help in the thickening process. It can be seen that the separation performance does not depend only on the geometry and operating conditions, but also on slurry concentration and particle size distribution. The concentration of the feed slurry and the operating pressure drop strongly affect the sharpness of separation.

KEY WORDS: Hydrocyclone, Solid-liquid system, Separation, Air-core

1. INTRODUCTION

Hydrocyclones are widely used in the mineral, chemical, coal, powder-processing industries for de-watering, or classifying according to a required particle size or density separation. The

reasons for this popularity lie in their simplicity of design and operation, high throughput, low maintenance, low operating cost and small physical size of the unit. Hydrocyclones are physically simple and robust separation devices with no moveable parts. A typical hydrocyclone consists of three sections; a cylindrical section, conical section and a tangential inlet section. The tangential inlet section is attached to the cylindrical section. The vortex finder is located centrally through the lid and at the top of the cylindrical section. Figure 1a shows a conventional hydrocyclone, which is inherently simple in construction. The design variables which influence the performance of the unit operation are the inlet and outlet diameters. The separation process is achieved as a result of the centrifugal force acting on the slurry and its components. However, there is a secondary flow down the outside wall of the vortex finder to the overflow, which is called a short-circuit flow. This flow was reported to cause low particle separation efficiency [1]. Svarovsky [2] suggested that a redesigned-vortex finder with a skirt can eliminate this inefficiency problem.

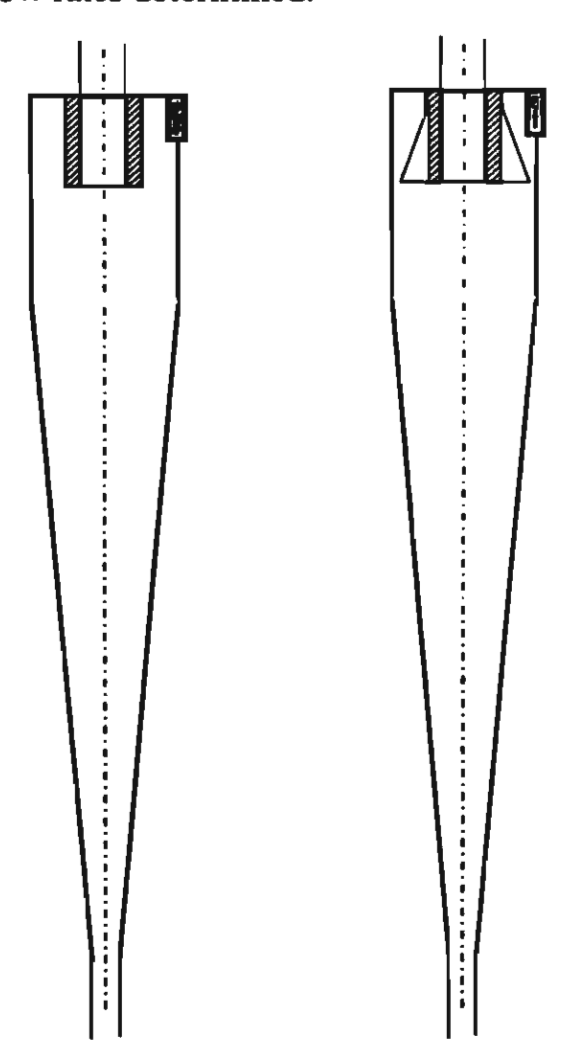
Despite its apparent simplicity, the elucidation of the mechanism of separation and detailed models of fluid flow with hydrocyclone separators has yet to be achieved. The main reasons for these short comings are: the complexity of solving Navier-Stokes equations for non-Newtonian anisotropic fluids that contain high concentrations of interacting particles, The complex high swirling and varying turbulence conditions prevailing in the separator, the presence of an interface (the air-core) inside the separator and the lack of on-online measurement methods to provide reliable experimental data for model development under credible process conditions [3].

An attempt to model the flow in a hydrocyclone has been made by using a theoretical model, which is based on solving the Navier-Stokes equations. This approach provides a physical insight into the fundamental causes of the observed phenomena. The earlier theoretical models were presented by [4], [5], [6], [7] and [8]. These steady state and 2D-axisymmetrical models have been considered, but the results are limited to dilute flow only. In addition, it is difficult to describe the behaviour of high turbulent swirling flow caused by the 3D flow entry. Therefore, more advanced modelling is needed that allows, for example, the study of such phenomena as an adjustment of three-dimensional flow to axisymmetrical, particle-fluid, particle-particle and particle-wall interactions. Such models will allow the description of particle effects on suppressing or generating turbulence and non-Newtonian slurry flows. Additionally, in the context of modelling turbulence, a physical model is needed to show how a fluid turbulent deformation characterises swirl flows and the deformation of the air-core inside the separator. Advanced theoretical and experimental techniques are needed to obtain a better understanding of the complex physical phenomena affecting the performance of hydrocyclones.

The purpose of this work is to study the flow behaviour, focusing on the air-core and underflow discharge characteristics, by using 50-mm transparent hydrocyclones with and without a vortex finder attachment (Fin). The experiments of these hydrocyclones treating CaCO₃ in water system are carried out. The knowledge of the underflow discharge characteristics relative to the operating pressure drop and feed property affecting the separation performance is investigated.

2. EXPERIMENTAL SYSTEMS

Figure 1 shows the schematic diagram of both 50-mm diameter acrylic hydrocyclones with and without a vortex finder attachment. They were equipped and set up with a feed pump and pressure gauge to measure the feed inlet pressure (see Figure 2). The vortex finder and apex diameters were kept constant at 14mm and 10 mm. Hydrocyclone overflows and underflows were directed back to the sump for recirculation. To study the flow behaviour and the characteristics of the air core, water was used. The operating pressure drop was varied from 10 psi to 35 psi by varying the inlet water flow rate. The density and the viscosity of water are 1031 kg/m³ and 1.330 cp, respectively. The size and the location of the air core were observed relative to the pressure drop. From each experiment, samples were collected from the feed, overflow and underflow streams. The collected samples were weighed and mass flow rates determined.



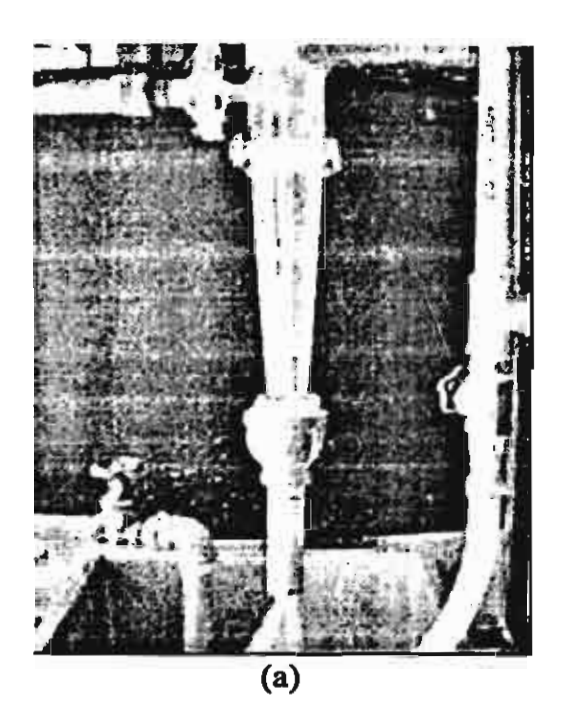
Geometry	Value (mm)
underflow internal diameter	10
vortex finder internal diameter	14
vortex finder outer diameter overflow	28
cylindrical section diameter	45
conical section length	270
cylindrical section length	40
width of inlet orifice	22
length of inlet orifice	40
height of inlet orifice	16
length of fin	6
height of fin	20

(a) (b)
Figure 1. Schematic diagram of 50-mm diameter acrylic hydrocyclones (a) conventional hydrocyclone and (b) with a vortex finder attachment (Fin).

The separation performance was examined by using the solution of CaCO₃ in water as feed slurry. The density of CaCO₃ is 2700 kg/m³. The flow rate and concentration of the feed was varied. In this case, the solid phase in each stream was also weighed to determine the concentration. The particle size distribution of each stream was measured by using the laser-diffraction size-analysis technique.

Overflow (return to sump) Pressure gauge Vortex finder Feed inlet Apex Underfloy Sump Pump

Figure 2. Hydrocyclone apparatus.



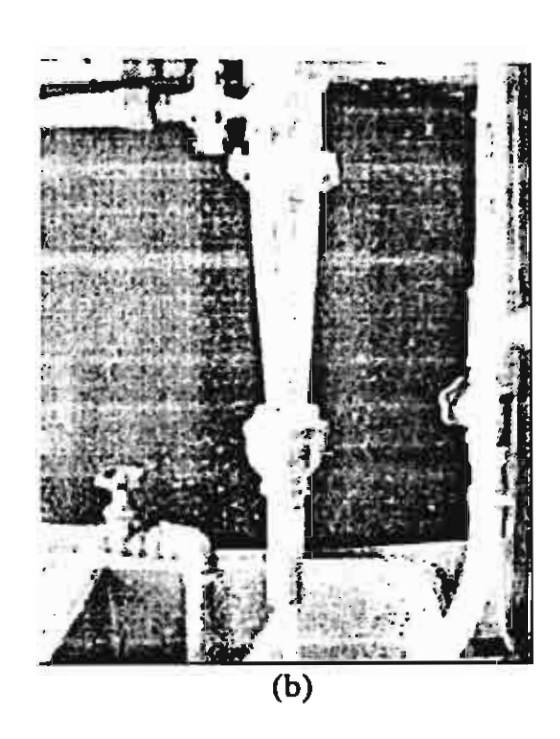
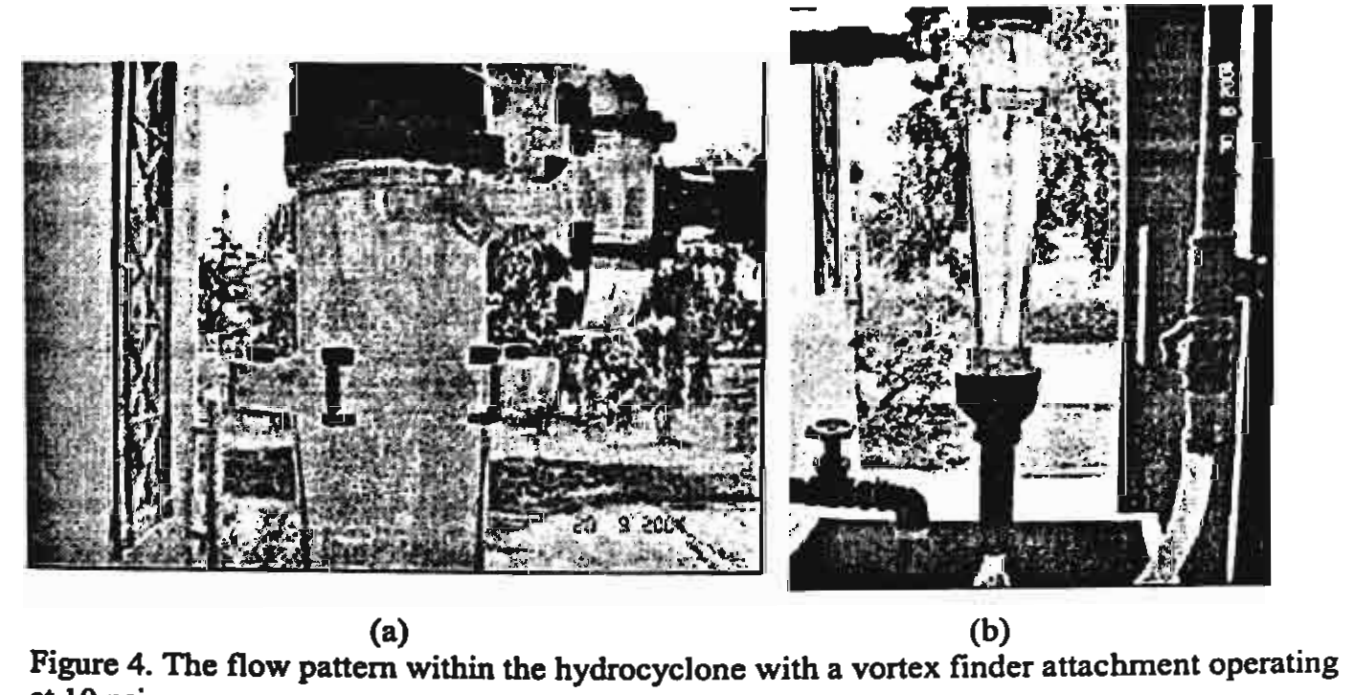


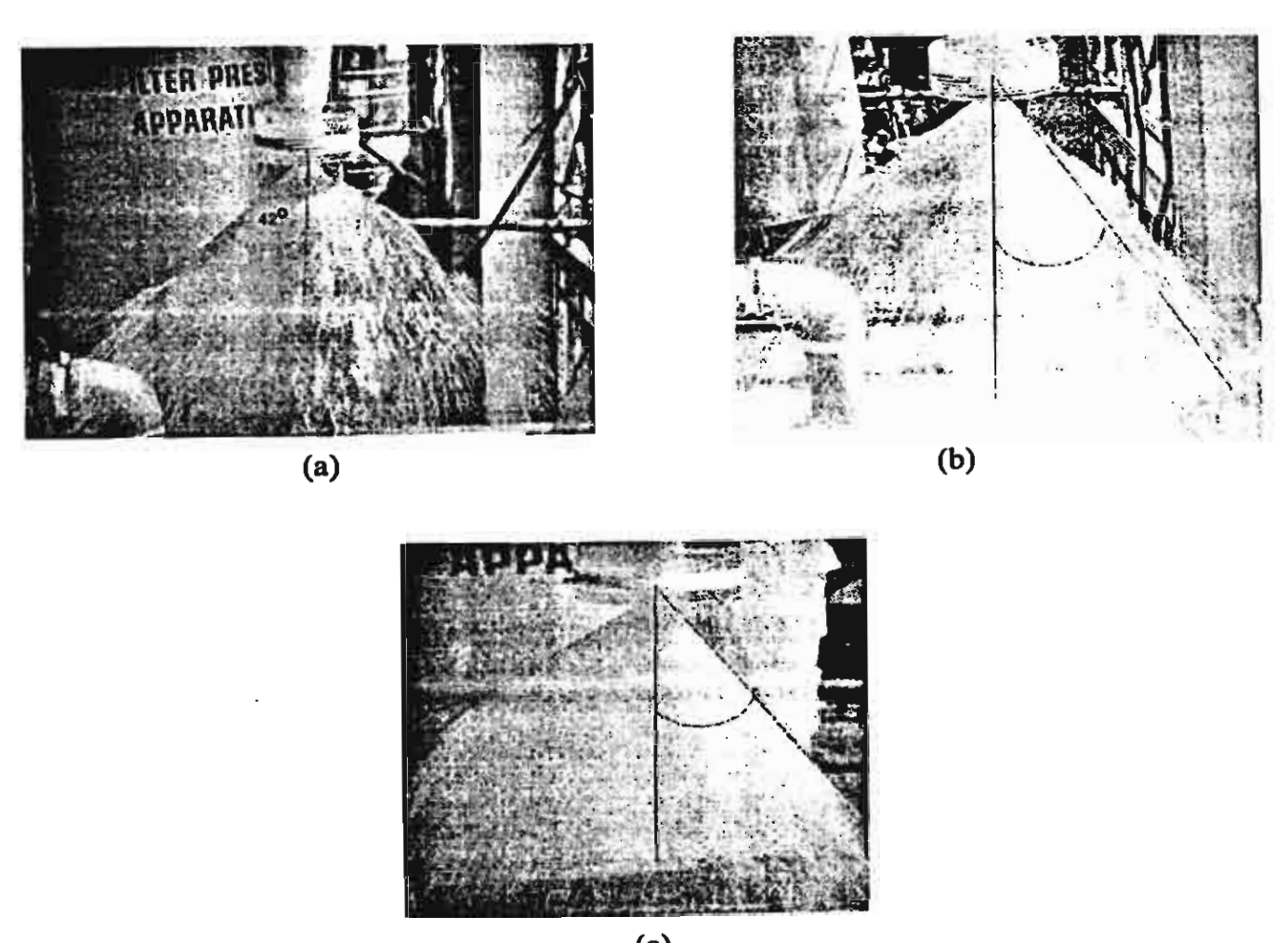
Figure 3. The flow pattern within the conventional hydrocyclone operating at: a) 10 psi b) 30 psi.



at 10 psi.

The diameter of the air-core of a conventional hydrocyclone for water-only flow was measured and found to be increased due to an increase in the pressure drop. It is also related to the angle of the underflow profile.

In addition, the angle of the underflow discharge of a conventional hydrocyclone treating CaCO₃ slurries was observed for 1%, 2% and 5% by volume of solid in feed as shown in Figure 5.



(c) Figure 5. The underflow discharge of the hydrocyclone operating at 30 psi for feed solid concentrations of: a) 1% b) 2% and c) 5% by volume.

A regular spray discharge from the spigot was observed in every experiment. The shape of the underflow discharge was found to be altered according to the change of feed-solid concentration and operating pressure drop as shown in Figure 6. Figure 6 also depicts the relationships between the air-core diameter, the angle of the underflow discharge and the pressure drop. It was found that an increase in pressure drop leads to an increase in the air-core diameter. However, in low-solid concentration cases, which are 1 and 2% by volume of

solid in feed, it was found that an increase in pressure drop leads to an increase in the angle of the underflow profile. For higher solid concentration, which is 5% by volume, it was found that above a certain operating pressure (25 psi), the discharge angle decreases due to the increase in pressure drop. This is due to the sedimentation of solids in the underflow section caused by high operating pressure in dense-flow separation.

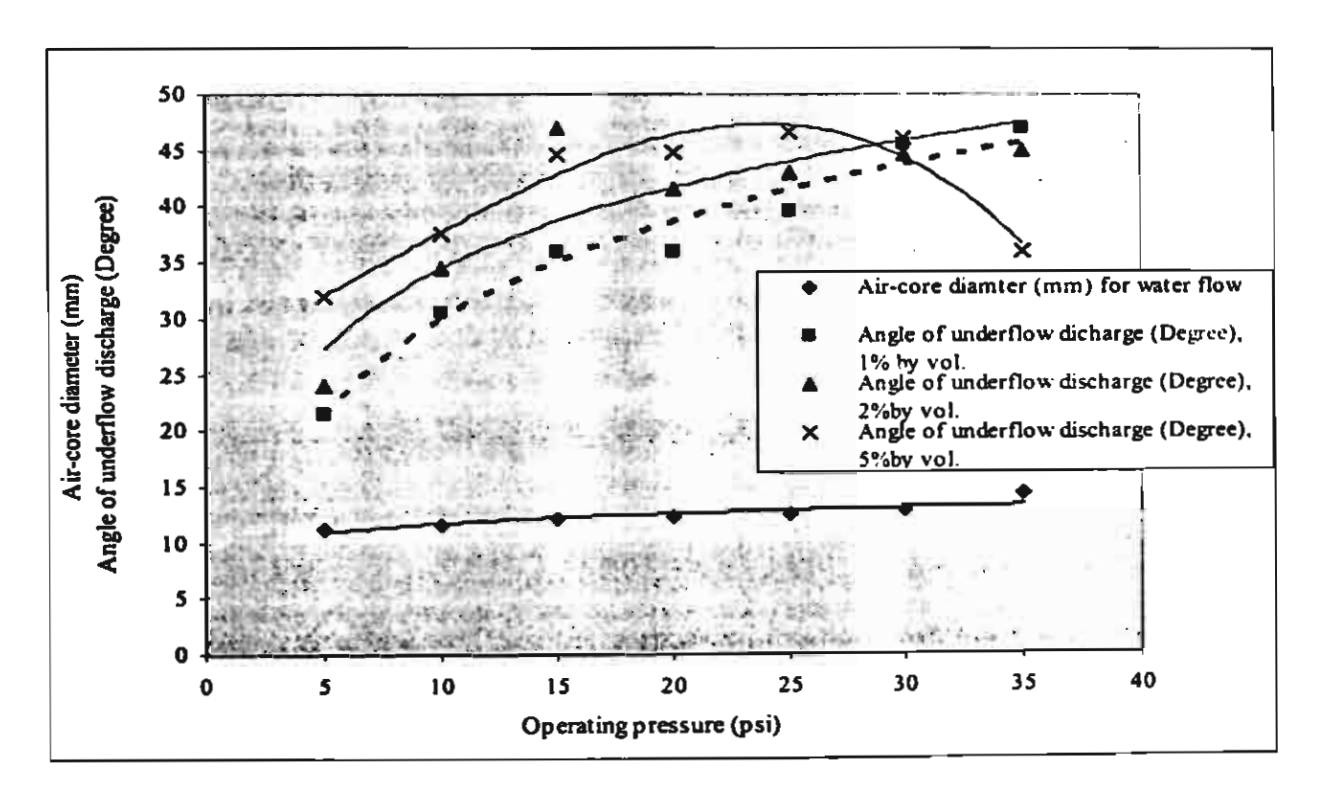


Figure 6. The relationship between the pressure drop, the air-core diameter and the angle of underflow discharge.

The solid concentration has a very strong effect on the angle of underflow discharge. The relationships between these three parameters are non-linear.

3. 2. Separation performance

The separation performance of this hydrocyclone with the extension pipe, treating $CaCO_3$ slurry, was examined. The operational data (pressure drop), the concentration and flow rate of each stream, the cut size and throughput ratio (R_f) of each test are shown in Table 1. The throughput ratio, R_f is the ratio between the volumetric flow rate of the underflow and that of the feed. The particle size distribution of the feed is shown in Figure 7. The selectivity curves are presented in Figures 8-11.

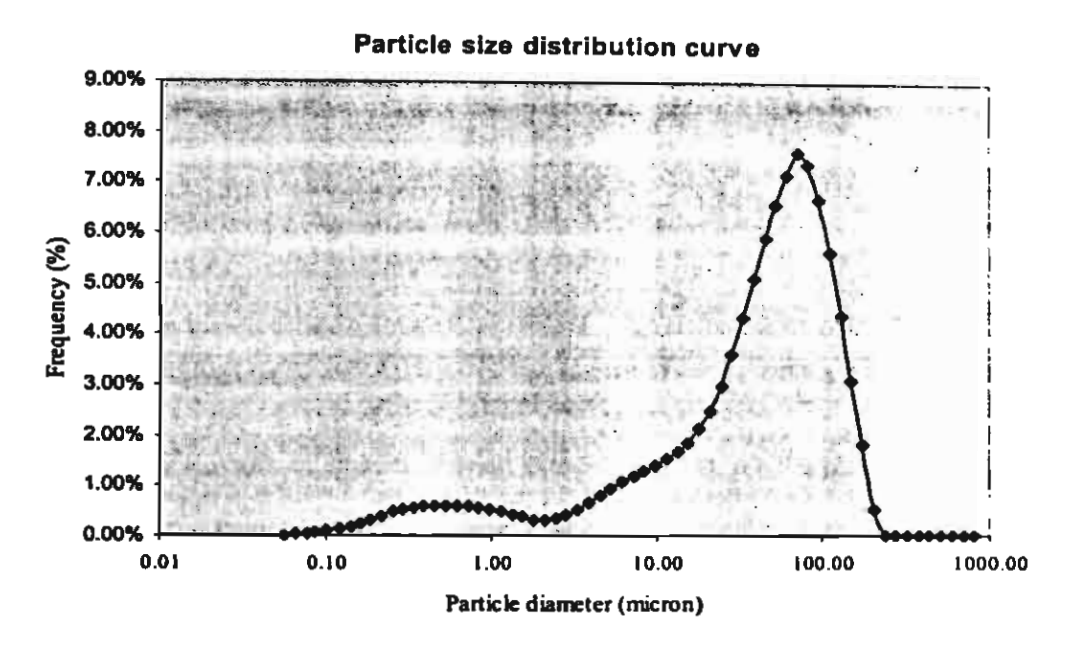


Figure 7. Particle size distribution curves.

Table 1. Experimental results.

Test Pressure		Feed		Over flow		Under flow		d _{so}	R _f
No.	Drop Δp (psi)	% by vol.	(gal/min)	% by vol.	(gal/min)	% by vol.	(gal/min)	- (μm)	
I	20	1	8.98	0.096	5.38	2.548	3.60	•	0.40
II	30	1	10.89	0.133	6.68	3.559	4.21	-	0.38
Ш	35	1	11.74	0.107	7.35	3.362	4.39	-	0.37
IV	20	2	8.64	0.207	5.08	5.088	3.56	-	0.41
V	30	2	10.53	0.218	6.54	6.321	3.99	-	0.38
VII	35	2	11.81	0.216	7.42	3.632	4.39	-	0.37
VII	20	5	8.47	3.030	4.91	11.340	3.56	40	0.42
VIII	30	5	11.28	3.415	6.93	14.163	4.35	11	0.38
IX	35	5	11.56	0.978	7.21	8.200	4.35	2	0.37
X*	30	0.20	9.62	3.74	3.15	3.95	6.47	-	0.67
XI*	30	0.37	9.32	0.78	1.45	3.92	7.87	-	0.84
XII*	35	1	10.01	0.22	3.62	0.87	6.39	-	0.64
XIII*	35	2	10.61	0.38	3.95	1.43	6.66	-	0.63

^{*} Hydrocyclone with vortex finder attachment (Fin).

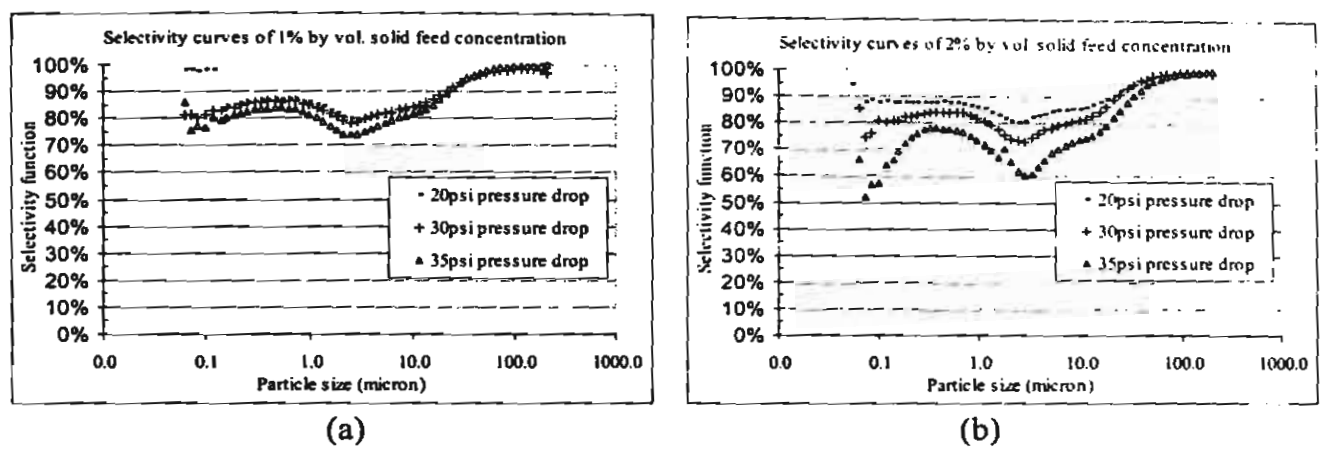


Figure 8. Selectivity curves of the feed solid concentration: a) 1% and b) 2% by volume for 20, 30 and 35psi.

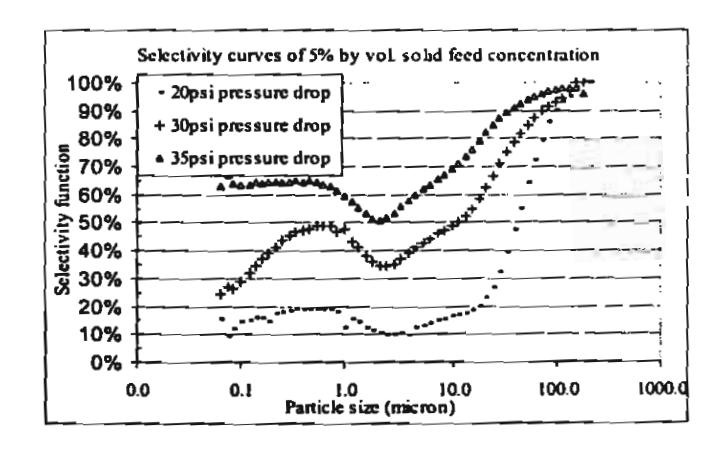


Figure 9. Selectivity curves of the feed solid concentration of 3% by volume for 20, 30 and 35psi.

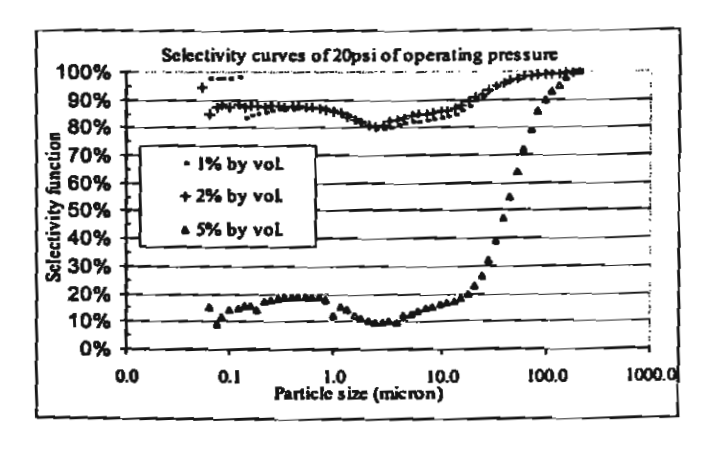
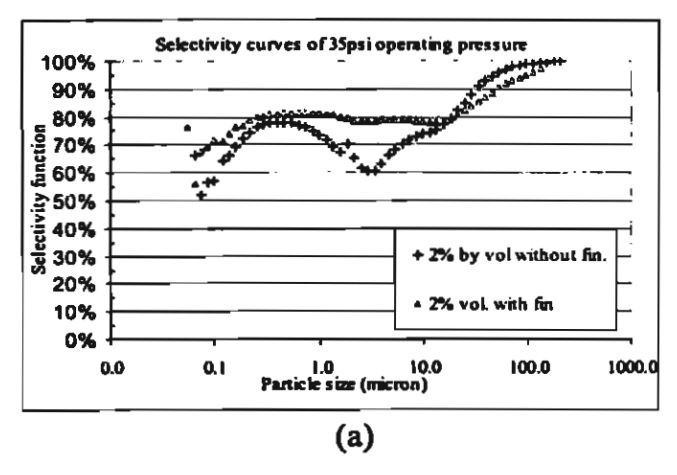


Figure 10. Selectivity curves of the operating pressure of 20 psi for 1, 2 and 5% by volume of solid in feed.



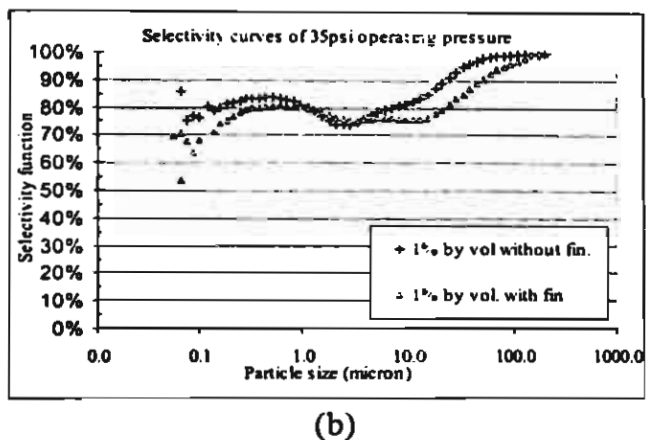


Figure 11. Selectivity curves of the operating pressure of 35 psi for: a) 1% and b) 2% by volume of solid in feed for the hydrocyclone operated with and without fin.

In this study, the operating pressure is limited. The highest pressure drop is 35 psi. In this range, it was found that the performance of the 50-mm hydrocyclone unit treating CaCO₃ slurry at 1 and 2% by volume was poor. The cut size cannot be obtained as can be seen in Figure 8a and 8b. However, the solid concentration in the underflow was three times higher than the concentration in the feed. The separation performance of the hydrocyclone treating the feed in this concentration range could be improved for a higher pressure drop.

The selectivity curves of the operation at the feed concentration of 5% by volume are shown in Figure 9. The separation performance of the hydrocyclone on this feed solid concentration is good. The results showed that the operating pressure of 35psi gave the smallest cut size. It is shown that the change in pressure drop obviously affects the hydrocyclone separation performance since an increase in pressure drop increases all velocities throughout the hydrocyclone. Therefore, an increase in pressure drop causes a decrease in the cut size.

The pressure drop used in practice usually depends on economic considerations. Operating at high-pressure means less units are required to treat a given flow. Lower capital costs, finer cut sizes and sharper separations can be obtained. These benefits must be offset against drawbacks including higher pumping cost and increased abrasion. Furthermore, the increase in feed flow-rate and the decrease in cut size tend to decline above a certain pressure drop. This is thought to be due to resistance effects within the hydrocyclone [9]. More details about the effects of the feed properties and the operational conditions on the separation performance can be found in [10].

The cut size of the 50-mm hydrocyclone unit treating CaCO₃ slurry also strongly depends on the feed concentration. It also appeared that the angle of the underflow discharge at an operating pressure of 35 psi was the smallest angle compared to those at 20 and 30 psi. The discharge of the separator contains the information which could possibly be used for better operational control, assuming that two distinct operational states of the hydrocyclone exist, which are the following: spray and roping. The states differ by the discharge profile from the

apex. Roping tends to form a rope-like discharge, while spray resembles an umbrella. Concha et al. [11] points out that the best separation occurs near the formation of rope discharge. Similarly, Neesse et al. [12] states on a broader note that a hydrocyclone achieves the best separation at a transitional discharge phase between roping and spraying. Therefore, with the calculation of the angle, determination of the operating performance of the hydrocyclone can be predicted. It is of interest to establish a procedure for improving the operation of hydrocyclones based on computational simulations.

A characteristic dip or fish-hook effect was observed in all experiments. It started to occur at particle sizes of approximately 2 microns. The analysis of this phenomenon is described in [10].

The separation performance of the hydrocyclone with the fin attachment was investigated for the feed concentration of 0.20, 0.37, 1 and 2% by volume. The results of the dilute feed (0.20 and 0.37% by volume) showed that the concentration of the underflow stream was ten to twenty times higher than that of the feed, but the selectivity curve showed low sharpness of separation and the cut size could not obtained. The fin attachment causes an increase in the throughput ratio. The results of the 1 and 2% by volume of the feed concentration showed very poor results as shown in Figure 11. The operation with 5% by volume of the feed slurry was also examined, and it was found that there was no overflow stream. This is due to the effect of the fin attachment forcing the flow swirling down to the apex tip and the high viscosity of the high concentration feed causing higher drag force, which reduces the effect of the centrifugal force. It can be summarised that the fin-type vortex finder attachment could not increase the sharpness of separation but it could help in the thickening process for a dilute feed system.

4. CONCLUSIONS

The results demonstrate that the air core is related to the type of underflow discharge and is a function of the pressure drop, which has an effect on the separation performance of the hydrocyclone. It can be seen that the separation performance does not depend only on the geometry and operating conditions, but also on slurry concentration. The results of this study are useful since they offer an ideal for improving hydrocyclone design and will assist in the validation of computational fluid dynamics (CFD) simulations.

5. ACKNOWLEDGMENTS

Acknowledgements are due to Ms. Nareerut Ju and Ms. Doungjai Tumma for experimental work and to the Thailand Research Fund for financial support.

6. REFERENCES

٨

- [1] Kelsall, D. F. "A study of the motion of solid particles in a hydraulic cyclone", Transactions of the Institution of Chemical Engineers, Vol. 30, pp. 87-108, 1952.
- [2] Svarovsky, L. "A short course in cyclones", Manual to Course at the Dow Chemical Co. in Freeport/Texas, January 10-11, 1994.
- [3] Bond, J., Cullivan, J. C., Climpson, N., Dyakowski, T., Faulks, I., Jia, X., Kostuch, J. A., Payton, D., Wang, M., Wang, S. J., West, R. M. and Williams, R. M. "Industrial monitoring of hydrocyclone operation using Electrical Resistance Tomography", 1st World Congress on Industrial Process Tomography Buxton, Greater Manchester, April 14-17, 1999.
- [4] Bloor, M. I. And Ingham, D. B. "Theoretical investigation of the flow in a conical", Transactions of the Institution of Chemical Engineers, Vol. 51, pp. 36-41, 1973.
- [5] Bloor, M. I. And Ingham, D. B. "Turbulent spin in a hydrocyclone", Transactions of the Institution of Chemical Engineers, Vol. 53, pp. 1-6, 1975.
- [6] Bloor, M. I. And Ingham, D. B. "The flow in industrial cyclones", J. Fluid Mech, Vol. 178, pp. 507-519, 1987.
- [7] Pericleous, K. A. and Rhodes, N. "The hydrocyclone classifier: A numerical approach", International Journal of Mineral Processing, Vol. 17, pp. 23-43, 1986.
- [8] Hsieh, K. T. and Rajamani, R. K. "Mathematical model of hydrocyclone based on physics of fluid flow", AIChE Journal, Vol. 37. No. 5, pp. 735-745,1991.
- [9] Bradley, D. "The Hydrocyclone", Oxford: Pergamon Press, 1965.
- [10] Kraipech, W. "Studying performance of industrial hydrocyclones", Ph.D. Thesis, UMIST, UK, 2002.
- [11] Concha, F., Barientos, A., Munoz, L., Bustamante, O. and Castro, O. "A phenomenological model of a hydrocyclone", in Claxton, D., Svarovsky, L. and Thew, M. (Eds), *Hydrocyclones '96*, London: Mechanical Engineering Publications Limited, pp. 63-82,1996.
- [12] Neesse, T., Schneider, M., Dueck, J., Golyk, V., Buntenbach, S., Tiefel, H. "Hydrocyclone operation at the transition point rope/spray discharge". In: Hydrocyclones 2004 in South Africa, 2003.